University of Stavanger

Faculty of Science and Technology

MASTER'S THESIS

Study program/ Specialization: Master of Science Petroleum Technology, Drilling	Spring semester, 2016 Open / ~~Restricted access~~
Writer: Alexander Brekke	Alexander Brekke (Writer's signature)
Faculty supervisor: Dan Sui External supervisor(s):	
Thesis title: Torque and Drag Friction Model: Implemented Friction Factor Dependency of Temperature	
Credits (ECTS): 30	
Key words: Torque, Drag, Friction, Friction Factor, Temperature, Model, ERD, ERW, Tribology, Regression	Pages: 110 + enclosure: 7 Stavanger, 15.06.2016 Date/year

Front page for master thesis
Faculty of Science and Technology
Decision made by the Dean October 30th 2009

Torque and Drag Friction Model: Implemented Friction Factor Dependency of Temperature*

Alexander Brekke

June 15, 2016

Abstract

We investigated the friction factor dependency of temperature. "Friction factor" is a parameter in the calculations of torque and drag. Increased well reach is dependent on accurate torque and drag modeling. We proposed that the friction factor can be dependent on temperature other than linear approximations as studied by Kaarstad et al. [2009]. The results was implemented in the work of Aadnoy [2006] torque and drag 3D model. The local friction factor in the wellbore was determined by a temperature model for local temperature in the wellbore and the result of the regression from the experimental work done with the tribology equipment in this thesis. We compared Aadnoy [2006] model with the nuances done to the model presented. The findings may lead to thorough research in the area of temperature and friction, and torque and drag models that are used today. Wellbore friction is an important theme in modern drilling in its search for increased well reach.

*This thesis is supported by help and guidance of Dan Sui, Tom Meling and Elise Graham. A special thanks to Mi-Swaco, and Line Forland for providing drilling fluids on our request.

Contents

Nomenclature

SECTION : 2

ERW	=	Extended reach well
HD	=	Horizontal displacement
TVD	=	True vertical depth
F_{up}	=	Pulling force
F_{down}	=	Slacking force
F_1	=	The bottom force of pipe element
β	=	Buoyancy factor
ΔL	=	Length of section
w	=	Weight per unit length
α	=	Wellbore inclination
μ	=	Friction factor
T_a	=	Drilling fluid temperature in annulus
$\theta_1, \theta_2, \alpha, \beta, C_1, C_2, A$	=	Model coefficients
x	=	Depth of interesting target
G	=	Geothermal gradient
T_s	=	Surface earth temperature

SECTION : 3

e_i	=	Residuals
y_i	=	Observed data
$\bar{y}$	=	Mean of the observed data
n	=	Sample size
p	=	Number of explanatory variables

SECTION : 4.1

σ	=	Normal stress
F	=	Force
A_a	=	Area
ϵ_s	=	Strain
ΔL	=	Change of length
L_0	=	Original length

E	=	Young Modulus
F_y	=	Tensile limit
F_a	=	Tensile limit, combined load
σ_y	=	Yield stress
SF	=	Safety factor
τ	=	Shear stress
σ_θ	=	Tangential stress
F_{sin}	=	Sinusoidal buckling
F_{hel}	=	Helical buckling
I	=	Moment of inertia
w	=	Weight per unit length
α	=	Angle of Inclination
r	=	Radius of drill pipe

$SECTION$: 4.2

m	=	Mass
F_n	=	Normal force
F_f	=	Friction force
ρ_s	=	Density steel
V	=	Volume of steel material
g	=	Gravitational constant
μ	=	Friction factor
β	=	Buoyancy factor
ρ_m	=	Density mud
ρ_{mo}	=	Density mud, outside drill pipe
ρ_{mi}	=	Density mud, inside drill pipe
r_o	=	Drill pipe radius outside
r_i	=	Drill pipe radius inside
Δs	=	Length of pipe
D	=	Outer diameter, drill pipe
d	=	Inner diameter, drill pipe
F_1	=	Force, previous element
F_2	=	Force, current element
w_{BHA}	=	Beoyant weight of bottom hole assembly
L_{BHA}	=	Length of bottom hole assembly
w_{dp}	=	Beoyant weight of drill pipe

L_s	=	Length of sail
R	=	Build radius
T	=	Torque
a	=	Horizontal length

SECTION : 4.3

θ	=	Inclination of force
F_t	=	Tangential force
P	=	Pressure

SECTION : 4.4

A_p	=	Cross-sectional area, drill string
N_{rep}	=	Reynolds number, drill string
A_a	=	Cross-sectional area, annulus
N_{rea}	=	Reynolds number, annulus
r_{bit}	=	Radius of drill bit
m_f	=	Flowrate
μ_{mud}	=	Viscosity of mud
N_{pr}	=	Prandtl number
h_p	=	Heat transfer coefficient, drill pipe
K_f	=	Thermal conductivity, drilling fluid
h_a	=	Heat transfer coefficient, annulus
U_p	=	Overall heat transfer coefficent, drill pipe
K_p	=	Thermal conductivity, drill pipe
U_a	=	Overall heat transfer coefficent, annulus
α_1	=	Heat diffusivity of formation
c_f	=	Specific heat, drilling fluid
ρ_f	=	Density, formation
t_D	=	Dimensionless temperature
t	=	Circulation time
T_d	=	Dimensionless temperature
$\theta_1, \theta_2, \alpha, \beta, C_1, C_2, A, B$	=	Model coefficients
r_{ci}	=	Radius, inside casing
K	=	Thermal conductivity, formation
T_{pi}	=	Temperature, inlet drill pipe

T_s	=	Temperature, surface
G_s	=	Geothermal gradient
H	=	Depth of well
T_p	=	Fluid temperature in the drill pipe
T_a	=	Fluid temperature in annulus
T_{max}	=	Maximum fluid temperature in the well
x	=	Depth of interesting target
q	=	Volumetric flow rate

1 Introduction

Modeling help us to understand the system in a drilling operation and predict future events; the knowledge is translated into a form that can be easily used by non-experts. Models related to drilling, such as the rate-of-penetration model, the fluid-property model, the fluid-temperature model, and the torque-and-drag model describe complex factors and unmeasurable variables.

Aadnoy [2006] presented a 3D friction model to determine torque and drag forces in the wellbore. The 3D model uses an average friction factor from the bottom of the drill string to the surface, measured by gathered field data, to determine the experienced friction forces: the average friction factor includes all the parameters that affected the friction factor throughout the well. It can only be determined by real-time torque and drag forces, which means it is only applicable in the post analysis of the well.

In the planning phase of the well, we use a modeled friction factor. The modeled friction factor is defined by laboratory experiments, and it is crucial to determine the local parameters that affect the friction factor in the wellbore to obtain equal value as the average friction factor which is seen in the post analysis. Kaarstad et al. [2009] modified the 3D model by introducing a modeled friction factor that was linear dependent of temperature. The friction factor increases proportionally to the increase of temperature.

The temperature increases with the depth of the well because of heat exchange from the formation. Therefore, a linear temperature model was used in Kaarstad et al. [2009] to determine the drilling fluid temperature at a desired depth in the wellbore. The result of the local temperature was used to determine the local friction factor.

The modeled torque and drag, based on the modeled friction factor used currently, is found to be dissimilar to the experienced real-time torque and drag in the field, based on the average friction factor. This gives theoretical justification to research the modeled friction factor. Experiment tests, which simulates a drilling process, are conducted at the laboratory with the tribology equipment to challenge the observations performed by Kaarstad et al. [2009], and see if we can locate other correlations between local friction factor and temperature. In determination of local friction factor the temperature is an important parameter, therefore an improved nonlinear temperature model will be used to determine the temperature of the wellbore fluids heated by the formation.

How could the result affect the torque and drag model?

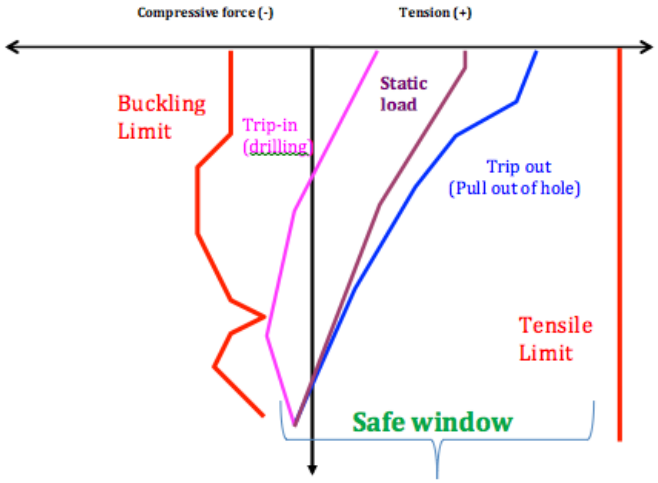

Figure 1: A safe drilling window is displayed between the two limiting forces; tensile and buckling limit. The friction forces are planned to be within the safe operational window Agonafir [2016].

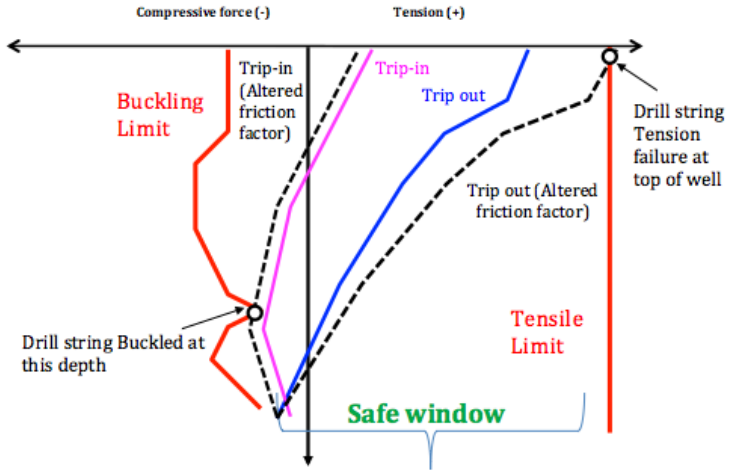

Figure 2: A different friction factor could lead to changed drag forces. Disastrous results such as failure of drill string may occur Agonafir [2016].

Knowledge of drill string mechanics is required to design a safe operation window. Torque and drag modeling calculates the friction forces that appear in the wellbore; such as trip-in, trip-out, and static weight, which are illustrated in Figures 1 and 2. The drill string capabilities are represented by tension and

compressive yield forces marked in red in the same figures. Any drag force that crosses the yield force will lead to failure of material and in the worst cases accidents such as stuck pipes and even blow outs. The drill string will either buckle by compression or experience tensile failure by tension.

The figures illustrate example drag forces that occur in various operations. In Figure 1, the drag forces modeled are accepted as they appear in the "safe window". The friction factor is a central part of torque and drag, and if the result of this research would lead to an altered friction factor, the drag forces would increase as well. This could be the difference of a successful drilling operation and a failed operation where human lives are in danger. In Figure 2, the trip-out and trip-in drag forces is illustrated with an altered friction factor. The drag force crosses the tensile and buckling limit, which leads to material failure. By performing research on the friction factor, we can participate in improved torque and drag modeling.

Contributions:

- By experimental approach, prove friction is dependent on temperature, Section 3.4.
- Claim that studies by Kaarstad et al. [2009] can be modified:
  - Apply a nonlinear temperature model to define wellbore temperature, Section 3.3.
  - Linear approximations vs non-linear approximations regarding increased temperature effect on the friction factor in drilling fluid, Section 3.4.
- Present a new friction model that implements the local temperature and friction factor in the wellbore: modifications on Aadnoy et al. [2010] 3D friction model, Section 3.4.

The thesis is written as a research paper. Proficient readers who are acquainted with drilling terms and definitions will be able to read the thesis without being distracted from the details. It is fascinating that the oil industry has accepted the general idea of friction being linear dependent of temperature, while there are many reasons to believe it could be nonlinear dependent. It is an unsolved problem that is presented in Section 2. Our idea based on experimental data gathered is accessible in Section 3 where it is compared to other people's approaches. Section 4 contains thorough presentation of torque and drag, friction, and temperature-topics that are relevant to the main idea of the thesis. The thesis also features a pilot on usage of tribology equipment in Section 5.

2 Research plan

Extended reach well

> The petroleum industry is on the brink of the golden days as we know it. Could extended reach drilling be the answer to the petroleum industry craves to reduce costs in future drilling projects?

Second to subsea installments, extended reach drilling evolution is the most important improvement in the oil industry. In regards of drilling wells from one platform instead of three, as area reach increases from each drilling station, environmental benefits, and potential production increase because of horizontal drainage. Realizing the vast investment of offshore production platforms, the advent of extended reach drilling is probably the single most important factor in cost minimization Aadnoy [2006]. For extended reach drilling the horizontal displacement is twice the length of the true vertical depth, given in Equation 1. Extended reach wells differ from original vertical drilled wells by drilling high angle wells and long horizontal sections, which become an engineering challenge.

$$ERW = \frac{HD}{TVD} > 2 \tag{1}$$

$$\begin{aligned} ERW &= \text{Extended reach well} \\ HD &= \text{Horizontal displacement} \\ TVD &= \text{True vertical depth} \end{aligned}$$

Extended reach wells have been drilled successfully for dozens of years, but the design is complex. Problems must be solved to be able to drill safely and reach farther targets, such as:

- Hole cleaning
- Mud design
- **Friction/Tribology**
  - **Torque and Drag**
- Lost circulation
- Wellbore instability

> "This evolution required new methods and technologies to be developed within borehole stability, well friction, mud and hydraulics, rig capacities and other technical areas." Regarding extended reach wells, Aadnoy et al. [2010] stated.

Torque and drag

For extended reach wells the strength of the drill pipe becomes of concern. Because of a long borehole the torque and the tension below the drill floor approaches the strength of the drill pipe. To be able to reach distances of 12 km and beyond, one has to minimize both torque and drag in the borehole Aadnoy [2006]. Torque and drag are limiting factors for extended reach drilling wells. Improved models have contributed to safe drilling and farther lengths. Johancsik et al. [1984] was first to introduce a torque and drag model in 1984. The models have since evolved to be more intelligent and accurate in regards to calculating the actual forces in the wellbore. From studies done by Mortensen and Brekke [2014], torque forces are greatly affected by friction and, in search of greater lengths, the torque overcomes the limits of the drill string capabilities. Frictional forces between the drill string and the borehole wall are what cause torque and drag. Models act as tools to drill efficiently to planned targets. Aadnoy et al. [2010] model provides a reasonable torque and drag prediction, and can be used in real-time analysis. The predictions assist in planning, operation, and post analysis to avoid drilling problems.

Torque is a result of force multiplied by arm. In a drilling operation, torque is the moment required to rotate the pipe. The moment should overcome the rotational friction in the well and the bit force against the formation. High drag and high torque are normally associated with each other. Torque is dependent of parameters; such as radius of the drill pipe, the friction factor, and the normal force.

Drag refers to friction forces that originate from tripping (lowering and pulling) of the drill string. It is the additional load compared to the free rotating drill string weight. Drag occurs because of contact friction with the formation in open holes or steel in closed hole scenarios.

Models are applied to analyze friction, in terms of a friction factor, to estimate how it affects torque and drag. In a typical extended reach well, which consists of a build and hold section, we differentiate between drag forces from the vertical section, the bend section, and the hold section. Bottom hole assembly is found at the bottom of the hold section. Bottom hole assembly consist of drill collars and tools. Above this point to the top of the sail, the drill string consist of drill pipes. The inclined well model is used to calculate the drag force in the hold section. In the bend section, the load on the drill string alternates between compressive and tensile loads. From studies performed by Johancsik et al. [1984] a non-linear first order differential equation is solved numerically, balancing between net force and the vector sum of the axial component of the weight to calculate the drag in bend section.

The tripping Equations 2-4 is found from Aadnoy et al. [2010] friction model in an inclined sail section. Friction is a part of the equations as the friction factor. In a drilling situation there are many situations where we have to trip-in and out of the wellbore, such as change of the drill-bit, installing casings or avoiding a pack off that results in stuck pipes. Indications of resistance appear on the real-time hook load when the drill pipe moves up and down in

the borehole. Equation 2 indicates forces that appear when the drill pipe is pulled. The pull force must overcome the force from the weight and the length of the drill pipe, and the friction force that appears between the drill pipe and the casing/formation. Equation 3 indicates lowering of the drill pipe. The friction force will act in the opposite motion. This example demonstrates how the average friction in Equation 4 can be discovered by hook loads for straight sections.[1]

$$F_{up} = F_1 + \beta \Delta L w(cos\alpha + \mu sin\alpha) \tag{2}$$

$$F_{down} = F_1 + \beta \Delta L w(cos\alpha - \mu sin\alpha) \tag{3}$$

$$\frac{\Delta F}{2} = \left[\frac{F_{up} - F_{down}}{2} = \frac{\beta \Delta L w(\mu sin\alpha)}{2} = Friction \right] \tag{4}$$

$$\begin{aligned} F_{up} &= \text{Pulling force} \\ F_{down} &= \text{Slacking force} \\ F_1 &= \text{The bottom force of pipe element} \\ \beta &= \text{Buoyancy factor} \\ \Delta L &= \text{Length of section} \\ w &= \text{Weight per unit length} \\ \alpha &= \text{Wellbore inclination} \\ \mu &= \text{Friction factor} \end{aligned}$$

Friction factor dependency of temperature

The coefficient of friction, μ, is a dimensionless scalar value that describes the ratio of the force of friction between two elements and the force pressing them together. The friction factor is an unmeasured complex function that is defined by parameters such as mud system lubricity, pipe stiffness, cuttings bed, stabilizers/centralizers, tortuosity, etc. The parameters vary over time and depth. The friction factor in open hole operations, such as drilling and liner installation, will vary from cased hole operations, such as completion and workover. A torque and drag analysis is therefore performed for different scenarios. To get an accurate friction model, an appropriate modeled friction factor is critical to define.

The friction factor has a significant impact in extended reach wells, as the wells are planned with increased measured length and a catenary profile. The direct consequence of this is more contact between the drill string and the casing/formation. The friction increases in such situations. In a catenary profile, the drill string will, in the horizontal/sail section, be forced against the side of

[1] Torque and drag model is discussed in more detail in Section 4.2.

the wellbore by gravity. Unlike in a regular vertical well, the drill string will hang in the center of the wellbore where it has less contact against casing/formation.

Torque and drag forces can be minimized by reducing the friction factor, increasing the ability to drill farther and deeper wells.

> "The minimization of friction in the well is one of the primary issues for these extended reach wells.
>
> Well friction is a critical parameter not only to drill the wells, but also during completion and work-over operations. The installation of the lower completion string in a long horizontal well is often one of the most critical operations. Therefore, knowledge and control of well friction is crucial." [Aadnoy, 2006]

> "State of the art torque and drag models do not include temperature effects. In practical applications one back-calculates one friction coefficient for the entire well, or separate cased and open holes. To obtain a good fit for measured data, unrealistic coefficients of friction must sometimes be used. Obviously the lack of realistic physics may lead to erroneous results. As a first step of developing more correct mechanistic models, we will now look into temperature effects." [Kaarstad et al., 2009]

The oil industry uses the simple one-parameter Couloumb friction model to analyze well friction, without including temperature effects. The coefficient of friction increases with temperature with nearly all fluids. It is shown in the study of Kaarstad et al. [2009] that the temperature effect on friction is considerable.

Friction between metals in air and water is severe; this friction is reduced significantly when drilling fluid act as lubrication between metals. There are different types of drilling fluid that are selected according to the operation, such as freshwater, saltwater, oil or synthetic, and pneumatic-based fluids. Each drilling fluid has dissimilar lubrication properties. The drilling fluid will have different local temperatures in the wellbore, that affect the lubrication and friction factor.

Drilling fluid, also called mud, is used in a drilling operation to maintain many functions:

- Clean the bit surface
- Transport cuttings
- Provide hydrostatic pressure against formation pressure
- **Act as lubrication to minimize friction**
  - Oil-based mud vs water-based mud
  - Lubrication depends on the type and quantity of drill solids and weight material + chemical composition.
  - Poor lubrication –> Increased friction –> High torque and drag –> Drill string failure

Oil-based mud is known as a better lubricator than water-based mud. This is because of the non-polar characteristics of oil, which allows particle attraction or repulsion. Water-based mud is an ionic fluid and is naturally charged. Oil-based mud reduces friction, but it is not environmentally friendly and recycling costs are high. There is a strong urge to research improvements in water-based mud. Additives limit increases in viscosity and gel-forming capability, as the chemicals react with water. Jahns [2014] studied the effect of nanoparticles (titania and silica) to increase lubricity in the water-based mud, acting as a ball bearing between metal surfaces. He concluded the research was a success regarding reduction of friction. Flow properties of a drilling fluid are strongly dependent on temperature and problems such as flocculation (shear rate increases) and dispersion (decrease in viscosity) begin to occur when a critical temperature is reached.

For a long time there was a lot of focus on how to minimize the temperature effects with improvements of the drilling fluid by implementing additives. In 1962, Ramsay introduced heat transmission approximation, and Holmes in 1969 introduced a temperature profile on drilling fluid in the wellbore. Knowledge of temperature in the wellbore became very critical in designing wells. The surface temperature of the drilling fluid is dissimilar to the temperature of the drilling fluid at the bottom of the wellbore, because of the geothermal gradient of the earth and the heat exchange to the wellbore, heated drilling fluid becomes nearly solid. Physical and chemical properties are affected by the temperature. The lubrication properties will change with the increase of temperature. Therefore, in the study performed by Kaarstad et al. [2009], the friction factor is presented as a linear function of temperature in equation 5. As the temperature of the drilling fluid increases with depth, the friction factor proportionally increases with depth. Each drilling fluid type acts differently to the temperature increase. Therefore, Kaarstad et al. [2009] presents friction factor equations for each drilling fluid.[2]

> "As the depth of the well increases, so does the temperature due to geothermal gradient of the earth. As wells get deeper, temperature slowly rises and it gets to a point which drilling fluid degradation occurs. " [Apak.E.C, 2006]

We will use the studies by Apak.E.C [2006] to determine the local temperature of drilling fluid in the wellbore and compare it with Kaarstad et al. [2009] assumption of temperature increase being linear with depth. Kaarstad et al. [2009] used a temperature model in their research, Equation 7, which included parameters, such as surface temperature, geothermal gradient, and depth. Apak.E.C [2006] introduced, Equation 6, a temperature model that also includes parameters, such as volumetric flow rate and circulation time. The Equations 6 and 7 is two ways of determining the annulus temperature and can be combined with Equation 5 to calculate the local friction factor in the wellbore at selected depth. The friction factor varies through the wellbore; therefore, it would be

[2]Friction is discussed in more detail in Section 4.3.

beneficial to use a discretization model to calculate the total drag and torque.[3]

Predicting the temperature profile of drilling fluid in a circulating well is dependent on the:

- Circulation rate
- Circulation time
- Fluid and formation density, specific heat and conductivity
- Fluid viscosity
- Drill pipe and annulus diameter
- Geothermal gradient
- Surface and inlet drilling fluid temperature

$$\mu = \alpha + \beta T_a \tag{5}$$

$$T_{a1} = \left(1 + \frac{\theta_1}{A}\right) C_1 e^{\theta_1 x} + \left(1 + \frac{\theta_2}{A}\right) C_2 e^{\theta_2 x} + Gx + T_s \tag{6}$$

$$T_{a2} = T_s + Gx \tag{7}$$

$$\begin{aligned} T_a &= \text{Drilling fluid temperature in annulus} \\ \theta_1, \theta_2, \alpha, \beta, C_1, C_2, A &= \text{Model coefficients} \\ x &= \text{Depth of interesting target} \\ G &= \text{Geothermal gradient} \\ T_s &= \text{Surface earth temperature} \end{aligned}$$

Research plan

The experimental work with tribology equipment[4], that is performed in this study, has a similar temperature range that appears in a typical extended reach drilling well. The temperature varies between 0-90 degrees. Temperature above this would only lead to dehydration of the drilling fluid and it would be more suitable for extremely deep wells. The research with tribology equipment is meant to confront the assumption of friction being linear dependent of temperature. A water-based mud will be tested multiplied times; the data gathered will be analyzed and a regression study will be executed to find the best fit to the results. A regression analysis is a statistical process for estimating the relationships among variables. We separate between linear and nonlinear regression.

[3] Temperature model is discussed in more detail in Section 4.4.

[4] Experimental friction measurements are discussed in more detail in Section 5.

The linear square method (Equation 5) is the line of best fit for data gathered. There are different options of nonlinear; such as the power model (Equation 8), the exponential model (Equation 9), the saturation growth model (Equation 10), and the polynomial model (Equation 11). In this thesis we focus exclusively on polynomial approach.[5] As Kaarstad et al. [2009], we will apply the modeled friction factor, μ, in the torque and drag model presented by Aadnoy [2006].

$$\mu = \alpha T_a^{\beta} \tag{8}$$

$$\mu = \alpha e^{\beta T_a} \tag{9}$$

$$\mu = \frac{\alpha T_a}{\beta + T_a} \tag{10}$$

$$\mu = \alpha_0 + \alpha_1 T_a + \ldots + \alpha_m T_a^m \tag{11}$$

Our aim is to study whether an extended reach well could be the solution to further decrease cost in the petroleum industry. As Aadnoy et al. [2010] states, well friction is one of the methods that should be developed and looked at again. This study modifies the models that have been used from the early stages of oil adventure.

[5] Use of ordinary least squares are unsophisticated models which can be performed with small population. Increased sophisticated models require numerious observations.

3 Results

The present report contains an investigation of the modification Kaarstad et al. [2009] presented to the theory of Aadnoy [2006]'s torque and drag model. The friction model is researched in terms of potential improvements and constraints. The theory of Aadnoy [2006] is implemented in Excel to provide an illustration of the main idea of this study; applying temperature-dependent friction. To study the effect of the experiment' results, three "field" cases have been applied with the friction model.

- Case study 1: Concerns the methodology of the friction model demonstrated with Example 7.1 from the book "Mechanics of Drilling" by Aadnoy [2006]. Demonstrate how the friction model is built by equations, function as a verification of the equations performed in Excel, and act as a foundation to which the results in case studies 2 and 3 can be related.

- Case study 2: Kaarstad et al. [2009] research, implemented with Apak.E.C [2006] temperature model. Demonstrate the importance of accurate temperature in the wellbore, which is used to determine the friction factor.

- Case study 3: "The friction factor correlation with temperature" results from regression analyses, implemented with Apak.E.C [2006] temperature model.

The main focus, where quality is essential, is the experiments performed with tribology equipment. The equipment is rare, and we are fortunate to experiment with it and seek for results that can be of great value for the petroleum industry. With such a lucky strike, we have not been fooling around with drilling fluid performed by guesses. We have brought in the best drilling fluid on the market. This drilling fluid is equipped all over the world in real drilling operations. With permission from Schlumberger's Mi-Swaco company, experts on drilling fluid, we have acquired drilling fluid which have the quality formula to perform thorough research; Glydril (water-based drilling fluid). Mi-Swaco and laboratory engineer Line Froland designed the drilling fluid to our specifications.

> "Mi-Swaco experience a difference in modeled (laboratory) and measured (offshore) torque and drag readings. In the laboratory the Glydril indicates a friction result different to how it appear in a real well. It has been difficult to get results with the water-based drilling fluid and its correlation to temperature. Better predictions of friction factor is important." Line Froland, MI-Swaco.

Mi-Swaco were intrigued by our idea to research another correlation between friction factor and temperature other than the linear correlation. It was recommended that we report back on the investigation performed.

The results from the experiment could be applied in a simulation program such as Wellplan. Wellplan is used in planning of well program in companies, such as Statoil. Verification of experiment: Real-time data like hook load

and torque readings from an actual drilling operation, can be compared to the simulations performed in the Wellplan, which would include the modifications discovered on the friction factor. This approach could present an indication of an improved friction model. This is recommended for future work.

As a result of, numerous assumptions that are necessary to generate an example well, Excel simulations will be sufficient to prove the idea. For the reader who is unfamiliar with the effect of a changed friction factor, simplified case studies are introduced to illustrate the effect.

3.1 Catenary well profile

Aadnoy [2006] summarizes the reasons for selecting catenary profile to an extended reach drilling due to its simplicity. The profile is traditionally used in deviated wells, where the well is vertical from the surface, than a kick-off with constant inclination creates a bend, before it is extended into the reservoir in a sail/horizontal section. The drill pipe capacity becomes of concern when the horizontal section is extended in long sections, one has to minimize the friction in the borehole. Torque and tension approaches the strength of the drill pipe. Friction can be reduced by adjusting different parameters; such as drilling fluid friction, dog-leg severity, bottom hole-assembly design, drilling fluid density and composition, and well path selection. The well path can be designed for minimum friction by selecting a catenary well profile.

3.1.1 Assumptions

- The wellbore is assumed to be smooth over the entire wellbore length, where shallow dog leg severity and tortuosity are not considered.
- The wellbore has constant build-up rates and drop-off rates for the curved sections.
- The friction factor modeled does not account for local variations in density and viscosity, and going from casing to open hole.
- A standard joint is used over the entire well profile.
- No azimuth change is assumed in the wellbore.
- A drilling operation is simulated; drilling fluid is the same inside and outside of the drill string.
- The analysis used, in regard input data, is done with reasonable and conservative values in mind.

The drill string is usually constructed with different drill pipes. An example is use of heavy weight drill pipes to provide weight and higher tensile strength than conventional drill pipes. Heavy weight drill pipes are often placed near the top of a long drill string for additional support. Aadnoy [2006]

General data	Drill string configurations	Well profile data/survey	Real time data/sensor values
Rig data	Drill pipe unit weight	Measured depth	Bit depth
Fluid properties	Drill pipe length	Measured inclination	Real time hook load
	Tool joint	Measured azimuth	Real time torque
	BHA unit weight	Casing shoe depth	
	BHA length		
	Largest radius in the BHA		

Table 1: Displays an example of input data that is related to any friction model Frafjord [2013].

3.1.2 Drilling data

Characteristic drilling data in Table 1 are utilized when performing simulation in any torque and drag model.

3.1.3 Well profile

The well is divided into three sections; a vertical section, bend section, and a sail section. There are many variations of well profiles that can be selected during well planning. The geologists and engineers decide a well profile that optimizes recovery, cost minimization, and safety. Extended reach drilling is associated with the well profile selected. This type of profile enhances recovery, it covers large horizontal displacement, and it is simple because of no inclination after the bend Mortensen and Brekke [2014].

The well sections are illustrated in Figure 3:

1. A vertical section from top-side to kick-off point, L_{KOP}.
2. A bend section from kick-off point to top of sail, L_B. The inclination, α, varies between 10-90 degrees with constant radius, R.
3. A sail section from top of sail that stretches to the target. L_S, put together by drill pipes, differ from L_{BHA}, put together by tools and drill collars.

We will use Aadnoy et al. [2010] 3D model to calculate an example well. The 3D model means it has the ability to calculate both inclination changes and azimuth changes. In the example well, the profile won't have any side bends. The azimuth changes will be negligible. Side bends are used when you have to bypass rough formation. The trajectory is only made by change in

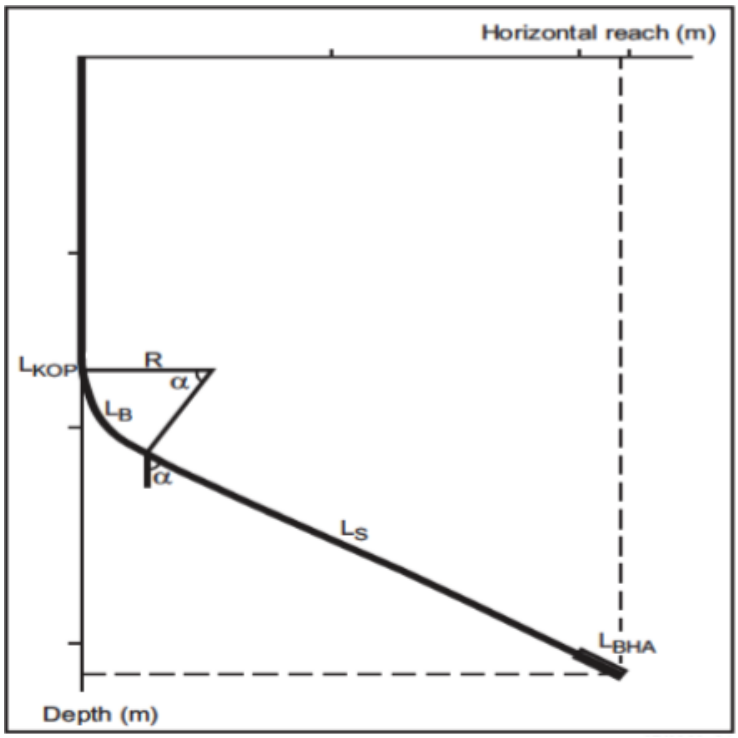

Figure 3: Illustrates catenary well profile in 2D plane: horiztonal reach and depth. The length of kick-off point, bend, sail section, bottom hole assembly are displayed together with the build radius and inclination of the well Aadnoy [2006].

inclination. Force calculation can either be calculated as a 2D model, a single plane, or we can set dog leg to become equal to inclination. Both options should give approximately the same solution Frafjord [2013].

3.1.4 Drilling fluid composition

> "The product contains other ingredients which do not contribute to the overall classification. Drilling fluid is a highly complex and variable blend of several proprietary products. Each drilling fluid is designed to meet the drilling requirements of a specific well. During the drilling process the composition and physical properties of the drilling fluid are constantly changing; therefore, a complete disclosure of a particular fluid's is impractical." Mi-Swaco.

Glydril Fluid properties	
Temperature	$50°C$
Plastic viscosity	$19cP$
Yield point	$24\frac{lbs}{100ft^2}$
Specific gravity	$1.56sg$
Rounds per minute	**Readings**
600	$62\frac{lbs}{100ft^2}$
300	$43\frac{lbs}{100ft^2}$
200	$37\frac{lbs}{100ft^2}$
100	$26\frac{lbs}{100ft^2}$
6	$10\frac{lbs}{100ft^2}$
3	$8\frac{lbs}{100ft^2}$

Table 2: Drilling fluid test results from viscosity and density equipment performed by Mi-Swaco.

Component	**Weight %- range**
Poly(oxy-1,2-ethanediyl), a-butyl-w-hydroxy	$5-10$
Crystalline silica (impurity)	< 1

Table 3: The composition of Glydril performed by Mi-Swaco.

Type	Nomenclature	Value
Kick-off depth	L_{KOP}	1500 m
Length, BHA	L_{BHA}	200 m
Buoyant Weight, BHA	w_{BHA}	3 kN/m
Length, Sail	L_S	2000 m
Build radius	R	500 m
Angle	α	60°
Buoyant Weight, Drill pipe	w_{DP}	0.3 kN/m
Mud density	ρ_m	1.56 s.g
Steel density	ρ_s	7.85 s.g
Buoyancy factor	β	0.8
Friction factor	μ	0.15
Radial clearance	r	0.08 m

Table 4: Input data.

3.2 Case 1: Average friction factor

The friction factor used is an average friction factor that is measured from the bottom of the drill string to the surface of the drill string. The average friction factor can be discovered by back calculations from real-time data, such as hook load and torque, in the post analysis of a well.

In planning of a well, we have to use an overestimation of the average friction factor to ensure that we account for all the parameters that will affect the friction factor. The value of the modeled torque and drag with average friction factor does not account for local variations, such as going from an open hole to casing, and temperature effects of viscosity and density. Therefore, by implementing average friction factor in planning of wells will lead inaccurate friction results, since the best result is an overestimation of the friction factor to ensure that the drill string will handle the friction forces that appear.

It is expected that the average friction factor is lower for operations, such as completion where the drill string is in contact with casing, than in a drilling operation where the drill string alternates between the casing and formation contact Frafjord [2013].

The average friction factor used for this case study is given in Mechanics of Drilling by Aadnoy [2006].

3.2.1 Input data

The input data in Table 4 is found in Mechanics of Drilling by Aadnoy [2006]. The input data is used throughout the result section, except for the friction factor, which is dependent of the experiment result from each case study.

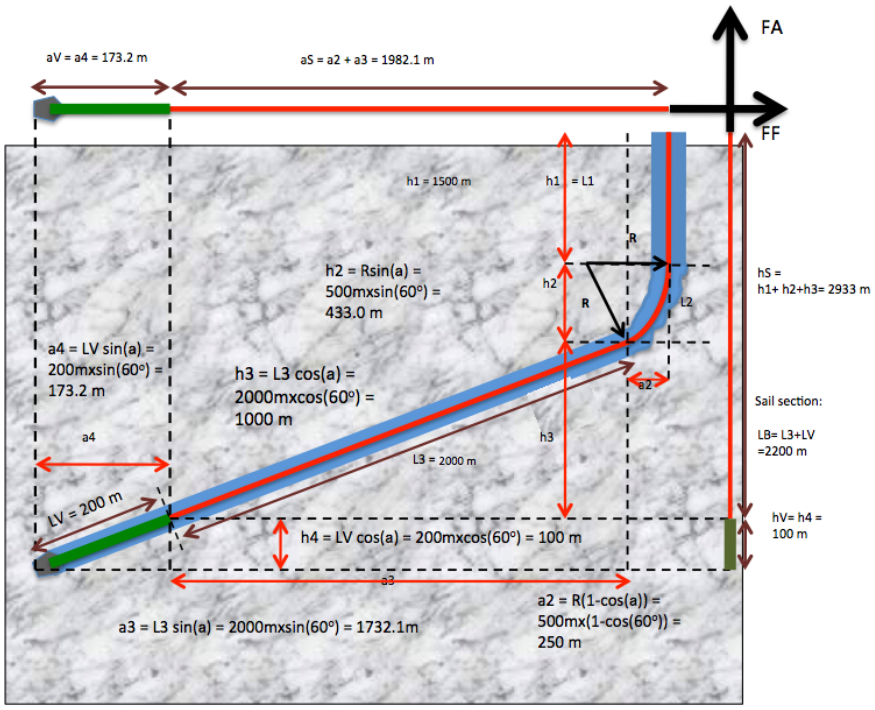

Figure 4: Depth calculations of the well.

3.2.2 Depth calculations

Depth calculations in regards of input data in Table 4 is included in Figure 4. The well are summarized in the horizontal plane $(a_2 + a_3 + a_4)$, vertical plane $(h_1 + h_2 + h_3 + h_4)$ and the total measured length $(L_1 + L_2 + L_3 + L_v)$ of the drill string. Summarized depth measurements from Figure 4 are presented in Table 5.

3.2.3 Well profile

The well profile is illustrated in 2D plane: horizontal displacement and true vertical depth. Kick-off point and build up are marked in the graphs where it is relevant to simplify the understanding of the different sections in the well. This illustration is used throughout the result section. The well profile is based on depth calculations performed in Table 5. As we can see from Figure 5, the well is vertical until it reaches the kick-off point at 1500 meters. The well is then with constant build up inclined by 60 degrees. A horizontal well is defined as 90 degrees. The well is then extended into the target area from the build up.

	Measured depth	True vertical depth	Horizontal displacement
Surface	0	0	0
Kick-off point	$1500m$	$1500m$	0
Top of sail	$2024m$	$1933m$	$250m$
Top of BHA	$4024m$	$2933m$	$1982m$
Bottom	$4224m$	$3033m$	$2155m$

Table 5: Displays the summarized depth calculations from Figure 4.

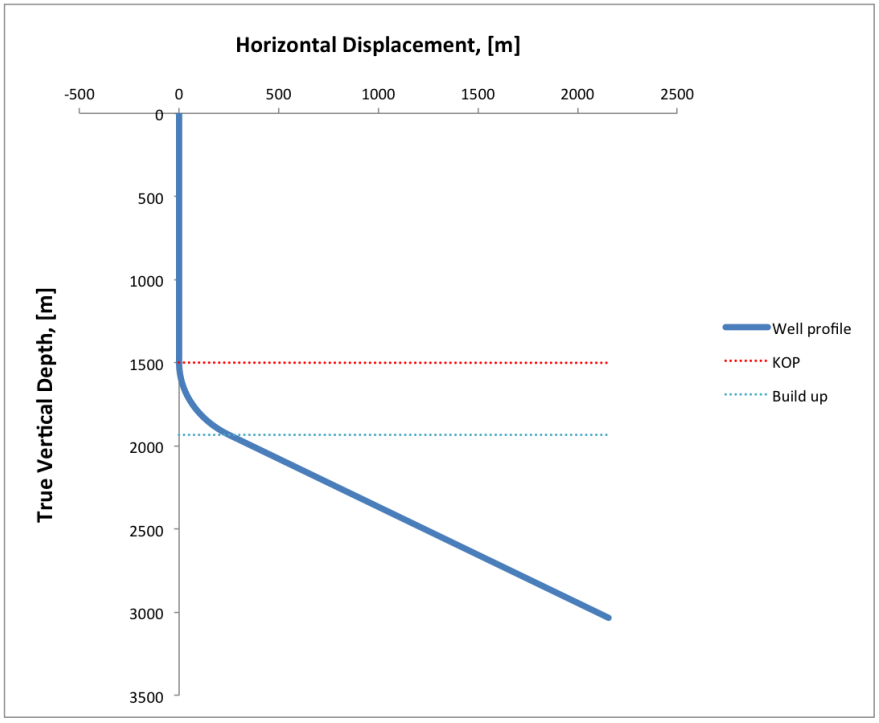

Figure 5: Well profile.

3.2.4 Hook load and torque

To control the forces that appear on the drill string when we rotate, pull, lower or keeps it static in the wellbore, the hook load and torque is determined. We can then use the load calculated and compare it to the limits of the drill string. The drill string must be able to withstand the hook load and torque, if the drill string capacity is not sufficient we need to do some adjustment to the planned well to ensure the loads are reduced.

When we are calculating the total friction force, we start from the bottom of the well. Then, we add the force from each element upwards. The force equations differ in: the sail section were they alternate between use of drill collars (bottom hole assembly) and drill pipes, at build up where inclination starts, and from kick-off point to the top of the well. The force at top of well is the total force that is expected in the system.

In this case study we introduce the following equations in Table 6 - 8 to determine total force for the various operations such as, static weight, pulling, and lowering. There are many friction models that have different nuances in how to calculate the friction force, but we have selected the friction model of Aadnoy [2006].

As we can see from Table 6, static forces are independent of friction factor. The drill string isn't moving; therefore there is no added friction to the system. The major difference between Table 7 and 8 is the motion of friction. When we pull the drill string, the friction acts against the motion, (therefore, downwards). This is represented by a $(+)$ sign in front of the friction factor in equations found in Table 7. It adds friction to the total force. Lowering equations indicate the opposite effect in Table 8. This is represented by a $(-)$ sign in front of the friction factor. The resulted hook load from the drag calculations in Tables 6-8 are plotted against the true vertical depth of each section in Figure 6. The horizontal lines represents the vertical depth of different stages in the well. As we expected, the total force at the top of the well is highest for pulling and lowest for lowering the drill pipe.

While we enter a well, the drill pipes are screwed together and tightened. Rotation of the drill pipe may break the connections by overextending the limit force. The limit is called make-up torque. The torque force calculated is ensured to be under the make-up torque of the drill string. As with drag equations, torque equations is also found from Aadnoy [2006]'s friction model. In Table 9, the calculations of torque from the case study input data are calculated. The calculations in Table 9 are shown in Figure 7. We can see from the figure that the well adds no torque from kick-off point to the top of the well.

We differ between drill bit off bottom called static torque, and drill bit against the formation, which adds to the total torque. In some situations it would be beneficial to rotate the drill string while pulling and lowering to avoid stuck pipe. In this case study we present the free rotational torque when the bit is located right above the bottom of the well in a static position, and rotation while pulling and lowering with drill pipe. By selecting drag force from pulling and lowering instead of static we get the result of torque in such operations.

Force	Equations, Drag-static weight	Fill in	Results [kN]
At Bit	$F_1 = 0$	$F_1 = 0$	0
Top BHA	$F_2 = F_1 + w_{BHA} L_{BHA} cos(\alpha)$	$F_2 = 0 + 3\frac{kN}{m} * 200m * cos(60)$	300
Top Sail section	$F_3 = F_2 + w_{DP} L_S cos(\alpha)$	$F_3 = 300kN + 0.3\frac{kN}{m} * 2000m * cos(60)$	600
At Kick-off position	$F_4 = F_3 + w_{DP} R sin(\alpha)$	$F_4 = 600kN + 0.3\frac{kN}{m} * 500m * sin(60)$	730
Top of well	$F_5 = F_4 + w_{DP} L_{KOP}$	$F_5 = 730kN + 0.3\frac{kN}{m} * 1500m$	1180
Total	$F_{total} = \sum_i^{n=5} F_i$		1180

Table 6: Demonstrate static weight calculations from the friction model of Aadnoy [2006].

Force	Equations, Drag-pulling	Fill in	Results [kN]
At Bit	$F_1 = 0$	$F_1 = 0$	0
Top BHA	$F_2 = F_1 + w_{BHA} L_{BHA}(cos\alpha + \mu sin\alpha)$	$F_2 = 0 + 3\frac{kN}{m} * 200m * [cos(60) + 0.15 * sin(60)]$	378
Top Sail section	$F_3 = F_2 + w_{DP} L_S(cos\alpha + \mu sin\alpha)$	$F_3 = 378kN + 0.3\frac{kN}{m} * 2000m * [cos(60) + 0.15 * sin(60)]$	756
At Kick-off position	$F_4 = (F_3 + w_{DP} R sin\alpha) e^{\mu\alpha}$	$F_4 = (756kN + 0.3\frac{kN}{m} * 500m * sin(60)) e^{0.15 * 1.047}$	1037
Top of well	$F_5 = F_4 + w_{DP} L_{KOP}$	$F_5 = 1037kN + 0.3\frac{kN}{m} * 1500m$	1487
Total	$F_{total} = \sum_i^{n=5} F_i$		1487

Table 7: Demonstrate pulling calculations from the friction model of Aadnoy [2006].

Force	Equations, Drag-lowering	Fill in	Results [kN]
At Bit	$F_1 = 0$	$F_1 = 0$	0
Top BHA	$F_2 = F_1 + w_{BHA}L_{BHA}(cos\alpha - \mu sin\alpha)$	$F_2 = 0 + 3\frac{kN}{m} * 200m * [cos(60) - 0.15 * sin(60)]$	222
Top Sail section	$F_3 = F_2 + w_{DP}L_S(cos\alpha - \mu sin\alpha)$	$F_3 = 222kN + 0.3\frac{kN}{m} * 2000m * [cos(60) - 0.15 * sin(60)]$	444
At Kick-off position	$F_4 = (F_3 + \frac{w_{DP}R}{1+\mu^2}((1-\mu^2)sin\alpha - 2\mu cos\alpha))e^{-\mu\alpha} + \frac{2\mu w_{DP}R}{1+\mu^2}$	$F_4 = (444 + \frac{0.3*500}{1+0.15^2}((1 - 0.15^2) * sin(60) - 2 * 0.15 * cos(60))e^{-0.15*1.047} + \frac{2*0.15*0.3*500}{1+0.15^2}$	511
Top of well	$F_5 = F_4 + w_{DP}L_{KOP}$	$F_5 = 511kN + 0.3\frac{kN}{m} * 1500m$	961
Total	$F_{total} = \sum_i^{n=5} F_i$		961

Table 8: Demonstrate lowering calculations from the friction model of Aadnoy [2006].

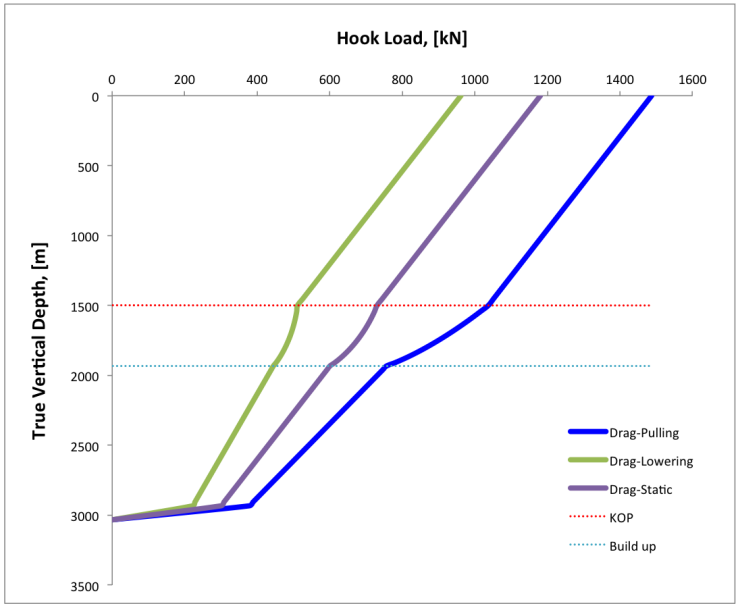

Figure 6: The calculated drag forces for each section are plotted against the true vertical depth. Kick-off point and build up is marked to simplify the understanding of the different sections in the well.

Force	Equations, Torque-static	Fill in	Results [kNm]
At Bit	$T_1 = 0$	$T_1 = 0$	0
Top BHA	$T_2 = T_1 + \mu w_{BHA} L_{BHA} r sin\alpha$	$T_2 = 0 + 0.15 * 3\frac{kN}{m} * 200m * 0.08m * sin(60)$	6.24
Top Sail section	$T_3 = T_2 + \mu w_{DP} L_S r sin\alpha$	$T_3 = 6.24kNm + 0.15 * 0.3\frac{kN}{m} * 2000m * 0.08m * sin(60)$	12.48
At Kick-off position	$T_4 = T_3 + \mu r * ((F_{3(static)} + w_{DP} R sin\alpha)\,\alpha + 2w_{DP} R\,(1 - cos\alpha))$	$T_4 = 12.48kNm + 0.15 * 0.08m * ((600kN + 0.3\frac{kN}{m} * 500m * sin(60)) * 1.047 + 2 * 0.3\frac{kN}{m} * 500(1 - cos(60)))$	23.45
Top of well	$T_5 = T_4$	$T_5 = 23.45kNm$	23.45
Total	$T_{total} = \sum_i^{n=5} T_i$		23.45

Table 9: Demonstrate torque-static calculations from the friction model of Aadnoy [2006].

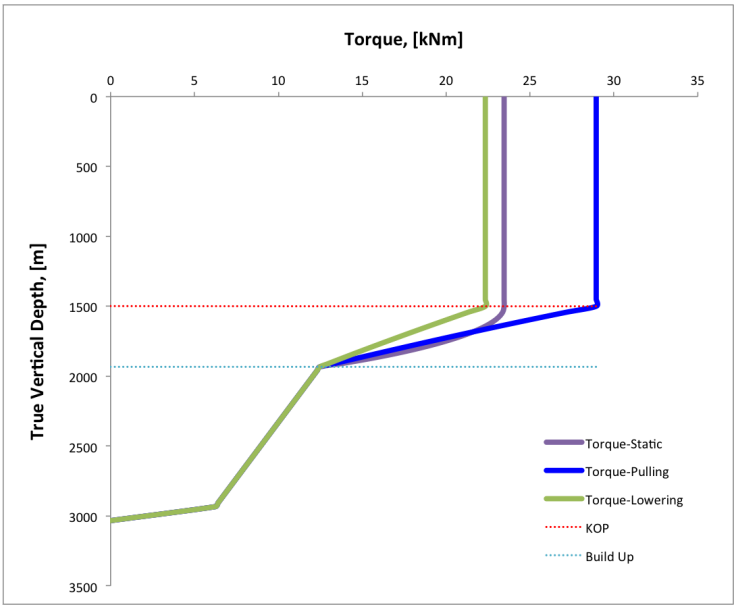

Figure 7: The torque calculations in Table 9 are plotted against the true vertical depth of each section. Kick-off point and build up is marked to simplify the understanding of the different sections in the well.

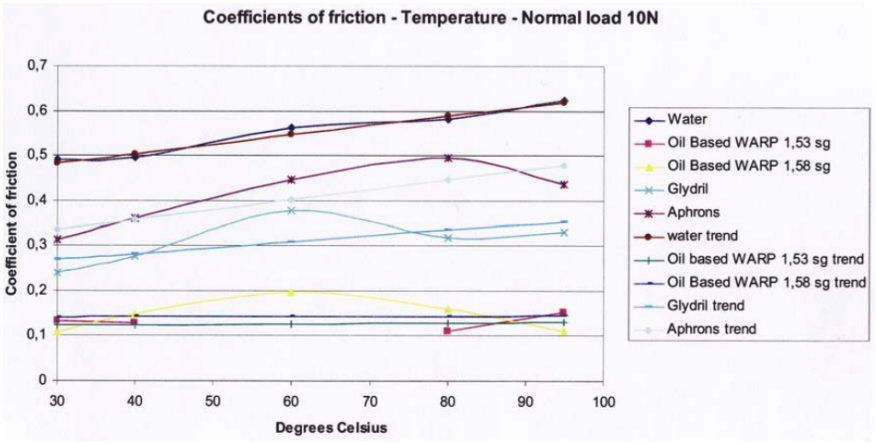

Figure 8: Reveals the research of Kaarstad et al. [2009]: how the friction factor varies with increased temperature. Different types od fluid are tested as a lubricator. Glydril is approximated to be linear, while it apparently seems to be nonlinear. This makes for an interesting research of the correlation between friction factor and temperature for this drilling fluid.

3.3 Case 2: Local friction factor determined by research of Kaarstad et al.

In case study 2 we introduce the modeled friction factor determined by experimental work at the laboratory. The modeled friction factor accounts for the local variations that appear in the wellbore. This differ from the overestimated static average friction factor used in case study 1. The friction model becomes more precise regarding calculation of torque and drag by implementing the dynamic friction factor, which is dependent of the temperature of the drilling fluid in the well. With these local variations in the friction factor, the modeled friction factor is less overestimated and more equal to the actual average friction factor found in the post analysis of the well.

Since the local friction factor is determined by the temperature that appear in the well, it is important that the temperature is accurately defined in the wellbore, this can be performed by applying a nonlinear temperature model, such as Apak.E.C [2006].

The friction factor correlation to the temperature in this case study, Figure 8, is determined by research of Kaarstad et al. [2009]. The dependent variable "friction factor" and the independent variable "temperature" are approximated to have linear relationship. We will contribute by modifying Kaarstad et al. [2009] research by implementing Apak.E.C [2006]'s investigation of drilling fluid temperature in the wellbore. The importance of accurate local temperature determination will be highlighted in this case study, as the temperature affect the found local friction factor considerably. The resulting friction factor from

the linear temperature model used in Kaarstad et al. [2009] study will be compared to the resulting friction factor from the nonlinear temperature model of Apak.E.C [2006] to illustrate the significance of accurate temperature predictions.

From Figure 8, the friction factor equations 12-16 are found by linear regression analysis. In this case study, we have selected the friction factor in Equation 15, Glydril, discovered by Kaarstad et al. [2009], to introduce the effect of Apak.E.C [2006]'s temperature model.

$$\text{Water} \rightarrow \mu_1 = 0.42 + 0.0021T \tag{12}$$

$$\text{Oil-based (1.53 s.g.)} \rightarrow \mu_1 = 0.12 + 0.0001T \tag{13}$$

$$\text{Oil-based (1.58 s.g.)} \rightarrow \mu_1 = 0.14 + 0.00005T \tag{14}$$

$$\text{Glydril} \rightarrow \mu_1 = 0.23 + 0.0013T \tag{15}$$

$$\text{Aphrons} \rightarrow \mu_1 = 0.42 + 0.0022T \tag{16}$$

3.3.1 Input data

Added input data are introduced to be able to determinate the annulus temperature. The input data selected is found from the fluid properties of Glydril and example data from the research of Apak.E.C [2006]. Reasonable and conservative values are selected. The friction factor is selected from Figure 8. The temperature model of Apak.E.C [2006] is created in US units, therefore the input data is prearranged to the model.

3.3.2 Annulus temperature calculation

The relevant temperature of drilling fluid in annulus is calculated to be able to determine the local friction factor in the well. Selecting the desired depth discovers the local temperature in the wellbore. Table 11 represents the equations from Apak.E.C [2006]'s temperature model and the calculated values used to determine the temperature of the annulus.

3.3.3 Annulus Temperature profile

Figure 9 shows two different approaches to calculate the temperature of the drilling fluid in the annulus, the nonlinear temperature model T_{a1} (Equation 6), and the linear temperature model T_{a2} (Equation 7). The temperature increases as the depth increases. This is due to the geothermal heat exchange to the wellbore. From the figure, the assumption of annulus fluid in the wellbore being equal to the geothermal gradient may seem to be an overestimation; thus resulting in an over estimation of torque and drag simulation by increased friction factor. It seems that the added parameters in the temperature model of Apak.E.C [2006] improves the accuracy of predicted temperature in annulus.

Type	Nomenclature	Value
Friction factor	μ_1	$0.23 + 0.0013T$
True vertical depth	H	$9950ft$
Drill string, outer radius	r_{o-dp}	$0.276ft$
Drill string, inside radius	r_{i-dp}	$0.266ft$
Drill bit size	r_{bit}	$0.349ft$
Casing, inner radius	r_{ci}	$0.427ft$
Flow rate	m_f	$12600\frac{gal}{hr}$
Temperature, drill pipe inlet	T_{pi}	$60°F$
Mud viscosity	μ_{mud}	$46\frac{lb}{ft*hr}$
Drilling fluid, thermal conductivity	K_f	$1\frac{Btu}{ft*F*hr}$
Drill string, thermal conductivity	K_p	$1\frac{Btu}{ft*F*hr}$
Drilling fluid, specific heat	C_f	$0.4\frac{Btu}{lb*F}$
Drilling fluid, density	ρ_{mud}	$13\frac{lb}{gal}$
Formation, thermal conductivity	K	$1.3\frac{Btu}{ft*F*hr}$
Formation, specific heat	C	$0.2\frac{Btu}{lb*F}$
Formation, density	ρ_f	$165\frac{lb}{ga}$
Temperature, surface	T_s	$59.5°F$
Geothermal gradient	G_s	$0.0127\frac{°F}{ft}$
Circulation hours	t	$44h$

Table 10: Added input data to the case study 2.

Type	Equation	Value
Cross-sectional area, drill string and annulus	$A_p = \pi r_{o-dp}^2$	$0,239 ft^2$
	$A_a = \pi(r_{bit}^2 - r_{o-dp}^2)$	$0.143 ft^2$
Reynolds number: drill string, annulus and prandtl number	$N_{rep} = \frac{\mu_{mud} C_f}{K_f}$	3434
	$N_{rea} = 0.816 \frac{2(r_{bit} - r_{o-dp})m}{A_a \mu_{mud}}$	1238
	$N_{pr} = \frac{\mu_{mud} C_f}{K_f}$	44
Heat transfer of drilling fluid, drill string and annulus	$h_p = 0.023(N_{rep})^{0.8}(N_{pr})^{0.4} \frac{K_f}{2r_{o-dp}}$	$127.58 \frac{Btu}{hr * ft^2 * ^\circ F}$
	$h_a = 0.023(N_{rep})^{0.8}(N_{pr})^{0.4} \frac{K_f}{2r_{bit}}$	$44.61 \frac{Btu}{hr * ft^2 * ^\circ F}$
Overall heat transfer of drilling fluid in drillstring	$U_p = (\frac{1}{h_p} + \frac{r_{i-dp}}{K_p} ln \frac{r_{o-dp}}{r_{i-dp}} + \frac{r_{o-dp}}{r_{i-dp} h_a})^{-1}$	$42.94 \frac{Btu}{hr * ft^2 * ^\circ F}$
	$U_a = h_a$	$44.61 \frac{Btu}{hr * ft^2 * ^\circ F}$
Heat diffusivity of formation	$\alpha = \frac{K_f}{c_f \rho_f}$	$0.0394 \frac{ft^2}{hr}$
Dimensionless temperature	$t_{D=} \frac{\alpha t}{r_{bit}^2}$	$14.2 > 1.5$
	$T_D = (0.4063 + 0.5 ln(t_d)) * (1 + \frac{0.6}{t_d})$	1.81
Model coefficient	$A = \frac{2\pi r_{o-dp} U_p}{\rho_{mud} m C_f}$	0.00114
Model coefficient	$B = \frac{2\pi r_{ci} U_a K}{(\rho_{mud} m C_f) * (K + r_{ci} U_a T_D)}$	$6.647E^{-05}$
Model coefficient	$\theta_1 = \frac{B + \sqrt{B^2 + 4AB}}{2}$	0.000326
Model coefficient	$\theta_2 = \frac{B - \sqrt{B^2 + 4AB}}{2}$	-0.000244
Model coefficient	$C_1 = \frac{-(T_{pi} - T_s + \frac{G_s}{A})\theta_2 e^{\theta_2 H} - G_s}{(\theta_1 e^{\theta_1 H} - \theta_2 e^{\theta_2 H})}$	-1.828
Model coefficient	$C_2 = \frac{(T_{pi} - T_s + \frac{G_s}{A})\theta_1 e^{\theta_1 H} + G}{(\theta_1 e^{\theta_1 H} - \theta_2 e^{\theta_2 H})}$	13.5
Temperature drilling fluid in annulus	$T_a = (1 + \frac{\theta_1}{A}) C_1 e^{\theta_1 x} + (1 + \frac{\theta_2}{A}) C_1 e^{\theta_2 x} + G_s x + T_s$	$135.88^\circ F$

Table 11: The temperature of the drilling fluid in annulus is calculated with the temperature model of Apak.E.C [2006].

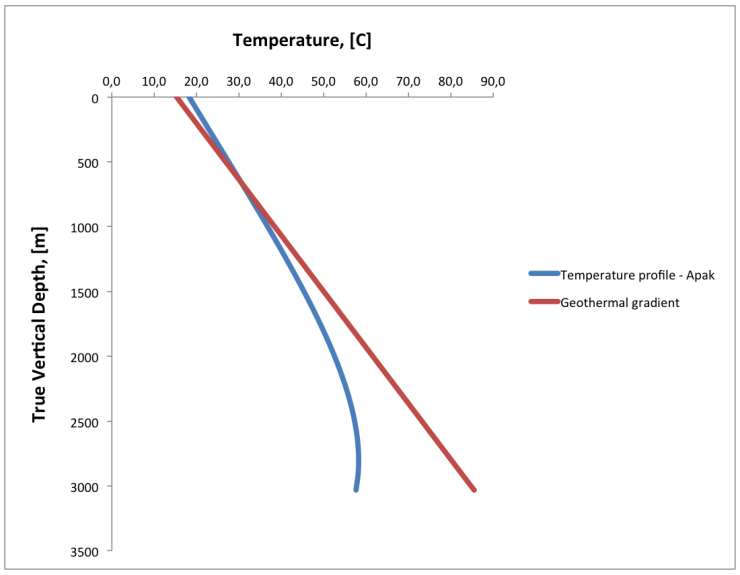

Figure 9: Shows two different approaches to calculate the local temperature of the drilling fluid in the annulus. Temperature is plotted against the true vertical depth of well.

3.3.4 Friction factor profile

Figure 10 is the result of the friction factor relation discovered by Kaarstad et al. [2009] with increased temperature. The temperature range in the figure is the temperatures found in the well by the model of Apak.E.C [2006]. As seen the local friction factor varies from 0.254 to 0.305 dependent on the temperature. The friction factor is lower at the top of the well, where the temperature found is $18°C$, while at bottom the temperature is $58°C$. From Table 12 we discover the increase in friction factor to be 19.1% from surface of the well to the bottom. From the table we also find the modeled temperature in annulus by the linear model. The local friction factor from top to bottom of well increases more with the linear temperature model, than with the nonlinear model of Apak.E.C [2006].

Figure 11 gives the relation between true vertical depth of the well and the friction factor. The same relation as the temperature of the true vertical depth is found in Figure 9.

Model	Depth	Temperature of drilling fluid in annulus	Local friction factor	Percent change
Apak.E.C [2006]	0	$20°C$	0.256	+19.1%
	$3033m$	$58°C$	0.305	
Geothermal gradient	0	$15°C$	0.250	+36.4%
	$3033m$	$86°C$	0.341	

Table 12: Illustrates the percentage increase in friction factor which is dependent of temperature. Temperature increase from the surface of the well and the bottom of the well.

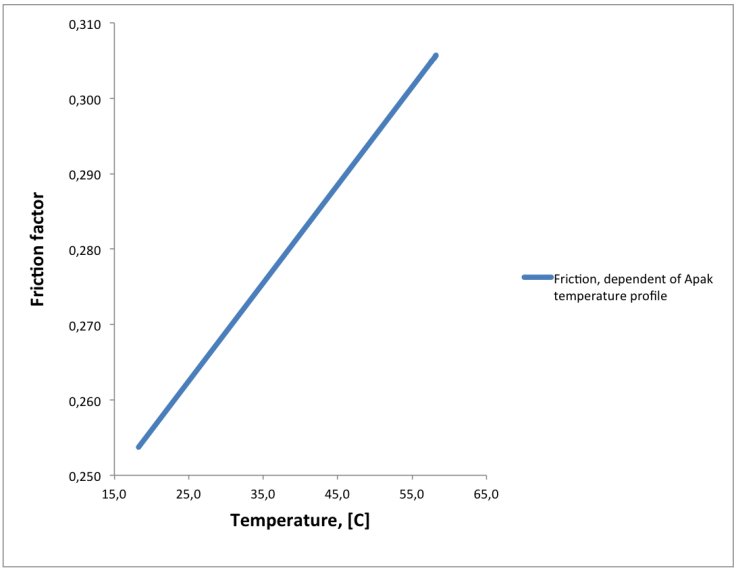

Figure 10: The linear correlation between friction factor and temperature is shown. The temperature range modeled in the annulus of the well is used as reference.

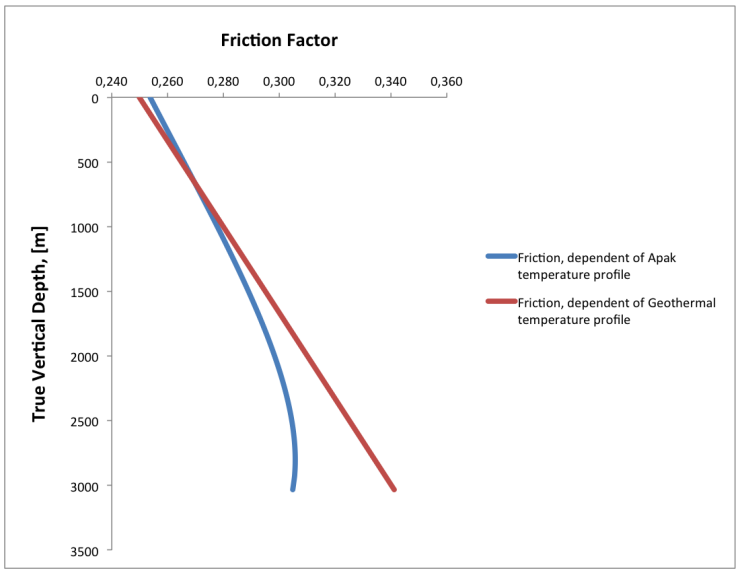

Figure 11: Expresses the local friction factor with glydril as lubriactor in relation to the true vertical depth. Two temperature models illustrates the significance of accurate predictions.

3.3.5 Hook load and Torque

The effect of temperature is essential to implement in modeling of torque and drag. The effect is seen in changes to the local friction factor in the well. To illustrate the effect, it is sufficient to introduce the changes in drag-pulling and drag-lowering, and the changes in the torque-static calculations to avoid the figures to be overcrowded by lines, and the meaning unclear.

Applying the nonlinear temperature model from Apak.E.C [2006] into the results from Kaarstad et al. [2009] indicates a better prediction of pulling and lowering. Pulling is reduced and lowering is increased, which implies improved prediction and less overestimation. This can be seen in Table 13.

Torque is also reduced with the nonlinear temperature model. In an extended reach well, reduction of torque is very important. From the studies of Mortensen and Brekke [2014], torque was found to be the limiting factor in the search of greater lengths. An accurate temperature model is proven to be essential when determining the friction factor: thus drag and torque forces.

Figure 12 and 13 demonstrates the proved point of the significance of accurate temperature predictions in the annulus.

Force	Apak	Geothermal	Percent change
Pulling	$186kN$	$191kN$	-2.6%
Lowering	$87kN$	$84kN$	$+3.5\%$
Torque-Static	$46kN$	$49kN$	-6.1%

Table 13: Demonstrates the effect of accurate temperature prediction in the wellbore.

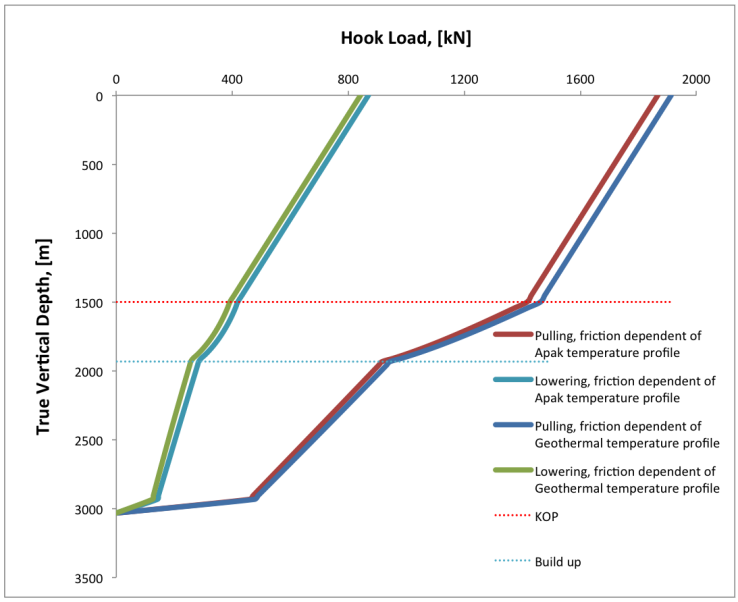

Figure 12: The drag forces are calculated with the different temperature models and plotted against the true vertical depth of the well. Kick-off point and build up is marked to simplify the understanding of the different sections in the well.

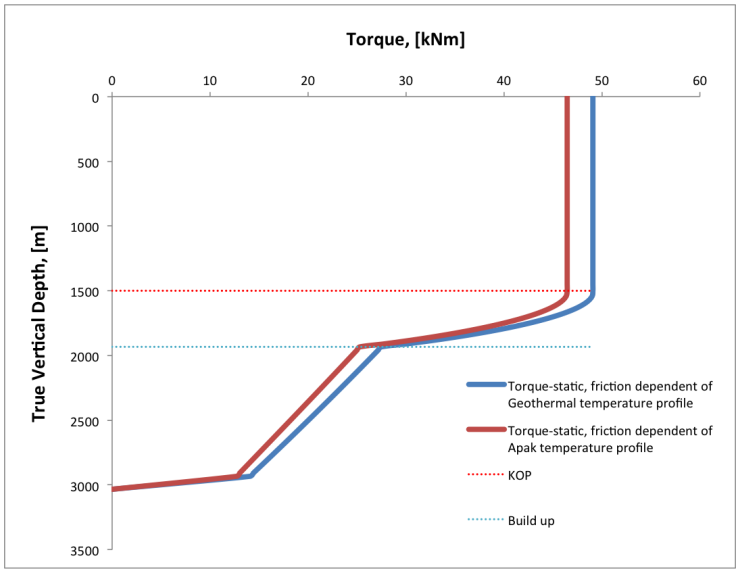

Figure 13: The torque forces are calculated with the different temperature models and plotted against the true vertical depth of the well. Kick-off point and build up is marked to simplify the understanding of the different sections in the well.

3.4 Case 3: Local friction factor determined by regression analysis from the experiments.

The experienced real-time torque and drag values are dissimilar to the modeled torque and drag values calculated in the well program. The average friction factor, used in case study 1, indicates an overestimation of the torque and drag values. The local friction factor correlation with temperature, in regard drilling fluid Glydril, found by Kaarstad et al. [2009] in case study 2 apparently seems nonlinear to the naked eye. This gives theoretical justification to research the local friction factor. The local friction factor, explained with a nonlinear model, may increase the precision to obtain an equal real-time average friction factor measured in the post analysis of the well, and therefore improve the torque and drag models.

The modeled friction factor from the laboratory needs to account for the same parameters as the measured average friction factor from the post analysis. The local friction factor is affected by temperature, which way it is affected becomes a really interesting discussion.

This leads us to study the findings by Kaarstad et al. [2009]. They have been very strict, in regards to the drilling fluid, Glydril in Figure 8, naming the correlation to be linear between temperature and the friction factor, while the line looks nonlinear to the naked eye. We base the result by Kaarstad et al. [2009] to be nonlinear due to the observations in the research doesn't appear to be in a line because of the observation at $60°C$, and that there is missing a regression analysis to indicate the result of it being linear. There are two arguments that are relevant to the result:

1. The true correlation between X and Y is nonlinear.
2. Or Kaarstad et al. [2009] experienced statistic noise with the gathered data either by:
   (a) the point at $60°C$ failed, and should actually be in line.
   (b) the two points above $60°C$ failed, and should actually be in line with the other points.

Because of the missing information regarding the data gathered and the regression analysis performed by Kaarstad et al. [2009] study, we have to assume one observation per degree in Figure 8; the result of this could lead to random coefficients occurring to the formula line. The thesis relative to Kaarstad et al. [2009] study, improves the research either by reducing statistics' noise to each degree or applying a nonlinear trend. Therefore, our analysis must be performed in the same way. At the outset, our study should be 100% equal to Kaarstad et al. [2009] study, we however, perform small modifications to search for new correlations, such as increasing the observations and search for a nonlinear correlation between temperature and friction factor. Keeping the other parameters in the experiment similar has therefore been prioritized. We increase the number of observations per degree, and use the average data to reduce the noise.

For comparability with Kaarstad et al. [2009], we collapse the observation into data averages for each temperature and run a regression analysis on the single average points. Summarized we will improve the research by Kaarstad et al. [2009] either by:

1. Support the result of Kaarstad et al. [2009], due to the five points becomes more precise, since they are an average of more observations.

2. Critique the result of Kaarstad et al. [2009], where we allow for different functional equations between the independent variable X and the dependent variable Y: the temperature and the friction factor.

We have decided to use ordinary least square models, such as polynomial of the 2^{nd} and 3^{rd} degree, as these can be directly comparable to the linear model . We do not have enough observations to perform 4^{th} and 5^{th} degree polynomial analyses, because it is not possible to have more variables than observations. With only five observations, we lose the flexibility in the estimation, therefore limiting our ability to perform other regression analyses. An alternative approach would be to collect observation from the entire temperature function and allow for more sophisticated regression methods, such as power, exponential, logarithmic, weighted least squares, etc. If the plan for the experiment was, for example, to perform sample tests to each integer of the temperature range $20 - 70°C$, we would get more observations and this would allow for more flexibility. A more sophisticated regression analysis could be applied. But, given the data material gathered, to acquire the same set up as Kaarstad et al. [2009], we are limited to linear and polynomial regressions.

3.4.1 Regression

Input data

To get reliable results from the experiments, the equipment was proper cleaned with ethanol bath to ensure no particle containment to the drilling fluid. All the parameters that affect the friction factor are attempted to be kept constant except the temperature, which is intended to vary. However, some parameters are difficult to manage because of limitations and some changes are unavoidable.

- Each material sample can be tested seven times before we have to install a new sample. Each installment leads to change of the drilling fluid. Therefore, heat exposure to the drilling fluid becomes inconsistent. This can affect the lubrication effect, as the drilling fluid has different lubrication stages. The new material contains a new surface and particle context even though the same material type is used.

- The tests creates wear track on the material sample, each test is performed at a clean surface on the material by increasing the radius of the rotational pin on disk. To ensure consistent parameters the linear speed is adjusted to keep the same rounds per minute.

Temperature	$30°C$	$40°C$	$50°C$	$60°C$	$70°C$
Test 1	0.372	0.225	0.285	N/A	0.3
Test 2	0.256	0.314	0.283	0.183	0.215
Test 3	0.132	0.291	0.245	0.214	0.272
Test 4	0.18	0.337	0.304	0.409	0.287
Test 5	0.409	0.254	0.277	0.359	0.389
Test 6	0.314	0.327	0.271	0.401	0.366
Test 7	0.301	0.272	0.316	0.345	0.313
Average	0.279	0.287	$0, .283$	0.3185	0.306

Table 14: Displays observations from seven material samples of steel performed with tribology equipment. The tests are performed with increasing drilling fluid temperature and the results are friction factors.

These parameters are creating variations in the observations, but applying average value of the sample test we cancel out some of the offsets. Besides these changes the other parameters are kept constant. The gathered data in Table 14 originates from seven material samples with the drilling fluid Glydril. Each sample is performed by increasing the temperature from $30°C$ to $70°C$, with increments of $10°C$.[6] This results in 35 observations. The average of the friction factor to each temperature is calculated for similarity to Kaarstad et al. [2009] study.[7] The results from the experiments are performed with steel against steel. This would simulate drill pipe in contact with casing situation.[8]

Figure 14 includes the test result from Table 14.

Regression analysis

We will determine which trend is better fitted to the gathered data: linear or nonlinear.

A brief introduction to regression terms is found in Table 15. The regression statistics of ordinary least squares regression are presented in Table 16. The values are used to determine which model is the best fit to the gathered experimental observations

[6] The equipment limited the research to $70°C$, because of evaporation and small sample holder.

[7] In test 1 at $60°C$, the result failed because of the equipment. Tracking of covered laps stopped in the middle of the experiment.

[8] A sample report of the experiments performed is included in the Appendix.

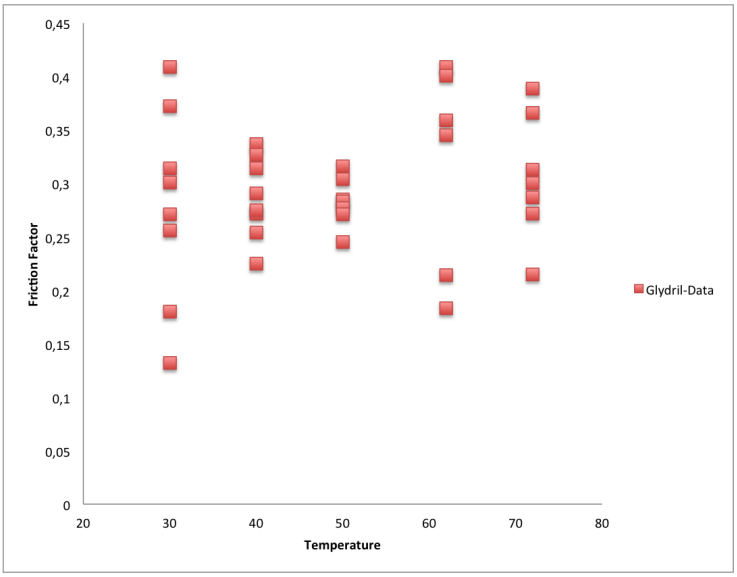

Figure 14: The gathered observations data in Table 14 are displayed.

Nomenclature	**Definition**
R	Measures how two variables move in relation to each other
R^2	Proxies how much variation in Y is explained by X in percentage
Adjusted R^2	Improved reliable statistics. It takes into account the number of variables in the regression. When you increase the number of variables it takes into account for the real increase in the explanatory power.
Standard error	Measures the variability of actual Y values from the predicted Y values
N	Sample size or population.
Line formula	Used to predict what is going to happen with the change in the X variable: in this case the temperature. The line formula will equal the change in the friction factor.

Table 15: Regression statistics explained.

	Linear Regression	**Polynomial Regression**	
Regression Statistics		**2.degree**	**3.degree**
R	0.79947	0.79942	0.87068
R^2	0.63915	0.63908	0.75808
Adjusted R^2	0.51886	0.27815	0.03232
Standard error	0.01164	0.01426	0.01651
N	5	5	5

Table 16: Regressions statistics calculated.

$$\bar{y} = \frac{1}{n}\sum_{i=1}^{n} y_i \tag{17}$$

$$e_i = y_i - f_i \tag{18}$$

$$R^2 = 1 - \left(\frac{\sum_i (e_i)^2}{\sum_i (y_i - \bar{y})^2}\right) \tag{19}$$

$$\text{Adjusted } R^2 = R^2 - \left(1 - R^2\right)\frac{p-1}{n-p} \tag{20}$$

e_i = Residuals
y_i = Observed data
$\bar{y}$ = Mean of the observed data
n = Sample size
p = Number of explanatory variables

Table 16 contains results of the regression analysis performed. We use the results to determine the model that describes the relation between the friction factor and temperature.

Line Formula

From the regression analysis we have found the line formula for the linear trend and nonlinear trend represented in the Equations 21-23. For comparison, the line formula for Equations 21 and 23 is introduced in Figure 15.

$$\text{Linear} \rightarrow \mu = 0.25231 + 0.00085T \tag{21}$$

$$\text{Poly } 2^{nd} \rightarrow \mu = 0.2513 + 0.00089T - 4.42857E^{-7}T^2 \tag{22}$$

$$\text{Poly } 3^{rd} \rightarrow \mu = 0.58088 - 0.02096T + 0.00046T^2 - 4.42857E^{-7}T^3 \tag{23}$$

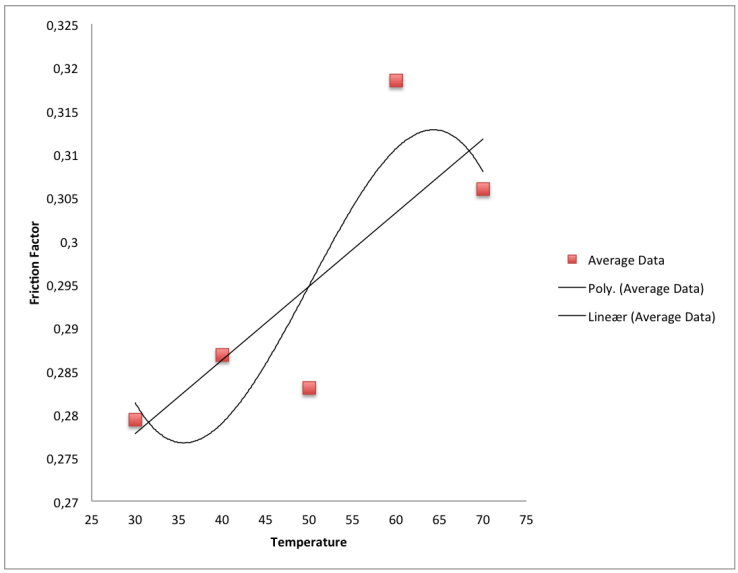

Figure 15: The average friction factor points is plotted against a linear and a nonlinear (3^{rd}polynomial) trend-line to illustrate the differences. The regression statistics can tell which model has the most explanatory power in relation to the observations.

Discussion

We have shown with Kaarstad et al. [2009] study, that the linear trend is questionable against the data. The linear trend can still be the true correlation, where the data is explained by statistical noise. In that case, we have improved the model by reducing noise with increased observation. The other alternative is that a nonlinear model is more suited to tell the correlation. Of the two hypotheses, where one supports Kaarstad et al. [2009], but still improves the result by reducing noise, or the second, which is a direct critique of Kaarstad et al. [2009] because the linear trend is not the true correlation, the discussion becomes which are the most suited to the regression analysis.

The coefficient of determination indicates how much variation in the response is explained by the model. The higher the R^2, the better the model fits your data.

$$R^2 \text{ increases in the order:} \quad \text{Linear} \rightarrow \text{ Poly-2.deg} \rightarrow \text{Poly-3.deg}$$

The R^2 order tells us that the model explains more of the Y variable for the 3^{rd} degree polynomial model; however, statistically, this becomes a misguided approach. The reason is, when we increase the number of variables, we automatically explain more of the dependent variable. For this reason, we investigate the precision of the model using the Adjusted R^2 parameter instead.

Adjusted R^2 increases in the order: Poly-3.deg $\rightarrow$ Poly-2.deg $\rightarrow$ Linear

Adjusted R^2 accounts for the number of predictors in your model and is useful for comparing models with different numbers of predictors.

So, with the right target, we discover that the linear model is the best fit. It has the most explanatory power and is the most accurate model to explain the observations according to the regression results.

We are satisfied with the analysis performed on these models, but there are other ways to perform the regression that include more models and increased polynomial degree. To be able to do these analyses the experiment must be performed in a non-comparable way to Kaarstad et al. [2009] study. The linear trend explains most of these regressions in this analysis, but there still exists the possibility that the other polynomials/models could explain the correlation in a nonlinear way. We still have the interesting findings in our result, which matches with Kaarstad et al. [2009], where the friction factor drops after the temperature at $60°C$. This requires increased data material in the form of observations. The success of this thesis, in form of results, is concluded to reduce statistical noise in the linear model.

As Kaarstad et al. [2009] proved, friction factor increases with temperature. This is also proved in our results with increased observations, which make the result more precise. An improved friction model could be created by implementing the improved local friction factor. The determination of the local friction factor can be used in all types of torque and drag models, such as Aadnoy [2006] and the mentioned Wellplan , which is used by Statoil. Further study of the friction factor is recommended to ensure correct specification of the correlation.

3.4.2 Hook load and torque

- Case study 1 introduced the well example, and the torque and drag model of Aadnoy [2006].
- Case study 2 introduced the temperature model of Apak.E.C [2006], and the significance of applying an accurate temperature model.

We will utilize the central topics in the case studies to present the main idea of this study. Work in the laboratory is completed, friction factor data are gathered at relevant temperatures of the drilling fluid given by Mi-Swaco, and a regression analysis is performed to present the friction factor correlation in this case study.

- We will present the best statistical fit model for the correlation between temperature and friction factor, which in the discussion is concluded to be the linear model, $\mu = 0.25231 + 0.00085T$.
- The temperature model of Apak.E.C [2006] will be used to calculate an accurate local friction factor in the well. Figure 16 represents the local friction factor at the desired depth of the example well.

- The local friction factor determined will be implemented in the friction model of Aadnoy [2006] to give an example calculation of torque and drag. The result of the experiments in the laboratory, if proven in an actual field operation, can be used in any torque and drag model.

Figures 17 and 18 introduce torque and drag friction model: implemented friction factor dependency of the temperature.

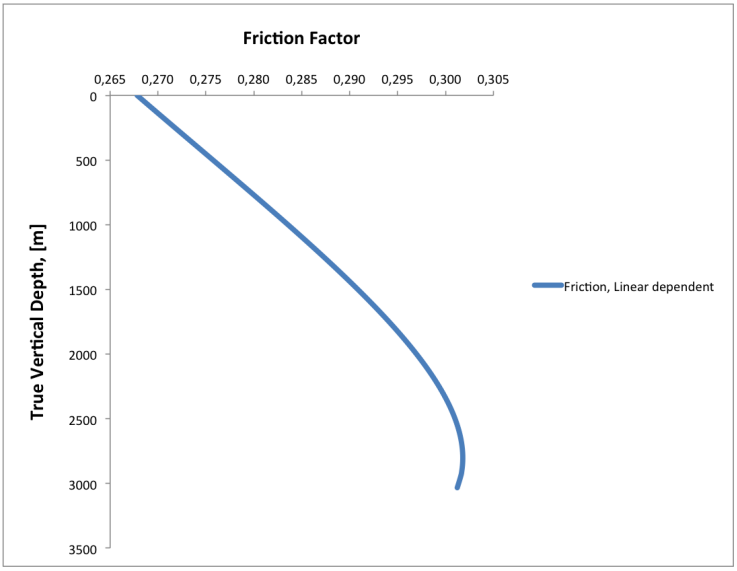

Figure 16: Expresses the local friction factor from the experiments on glydril in relation to the true vertical depth. Temperature model of Apak.E.C [2006] is used to determine the local temperature in the wellbore.

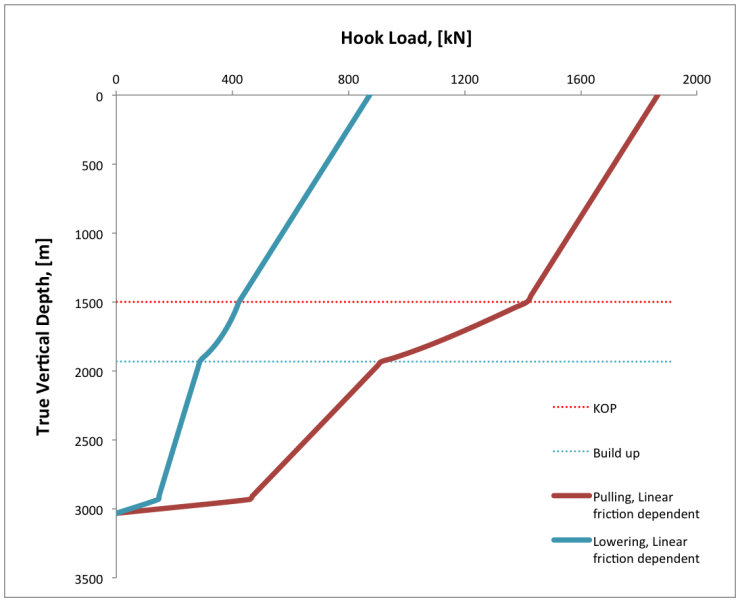

Figure 17: The hook load is calculated with the experimental result, the linear approximation is used to determine the local friction factor, with the temperature model of Apak.E.C [2006].

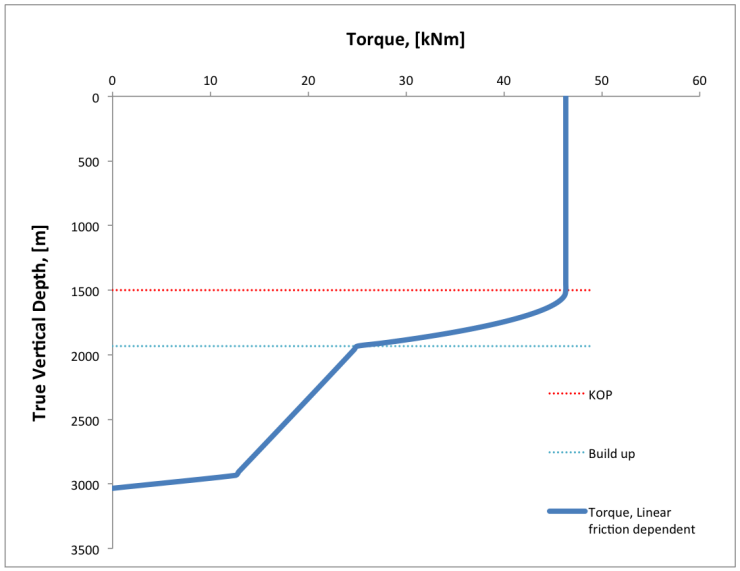

Figure 18: Torque-static is calculated with the experimental result, the linear approximation is used to determine the local friction factor, with the temperature model of Apak.E.C [2006].

4 Fundamentals

A thorough introduction of the fundamentals presented in the thesis is found in the following subsections. The main topics are: the drill string capabilities, torque and drag, friction, and temperature in a wellbore.

4.1 Mechanics of drilling

Knowledge of the drill string mechanics is used to create a safe operational window in the planning phase of the well. It is important that the drill string can handle the loads, which are expected to appear in pulling and lowering of the drill string. In a drilling operation, it is crucial to be aware of the drill string capacity. Extending the drill string capacity would lead to failure of the drill pipe either by compression or tension. The failure limits are called buckling and tensile limits. Applying torque to the drill string will give torsional force. Each stand of the drill pipe is made up to a certain make up torque when they are connected. This is the torque limit the drill sting can handle before it twists off.

Mechanics of materials is an analysis of internal forces (stress) and solid deformation (strain) under different loadings. In a drilling, completion, and workover operation axial and torsional loading is applied on the drill string and deformation occurs. The drill string elongates by tension and deforms by compression. With good planning, drill string problems, drill bit problems and formation related problems can be avoided. Total abandonment could be the result if a serious problem occurs Agonafir [2016].

4.1.1 Operational window

In the pre-phase of a well operation, it is required that a safe operational drilling window is introduced to the well program. A thorough operational window supports a well to drill safely to a target. In cases were the torque and drag forces extend the safe drilling window, we could end up with a stuck pipe and a fishing job. Once the safe drilling window is designed, it can be used against real-time monitoring. In Figure 19, a safe drilling window is created and if all goes to plan in drilling operations, the well will be a success in regard to drill string mechanics. In cases where the experienced drag force is higher than expected, tensile failure of the drill string may occur. In a operation of slack-off/lowering, the drill string is in compression and the pink line crosses the buckling with torque limit. Pulling of the drill string crosses the tensile limit Agonafir [2016].

4.1.2 Tensile Limit

Stress is defined as force per unit area. Normal stress is perpendicular to the plane face and shear stress is parallel to the plane. Given axially load and cross-sectional area, the stress and strain can be calculated with mechanics of materials derivation:

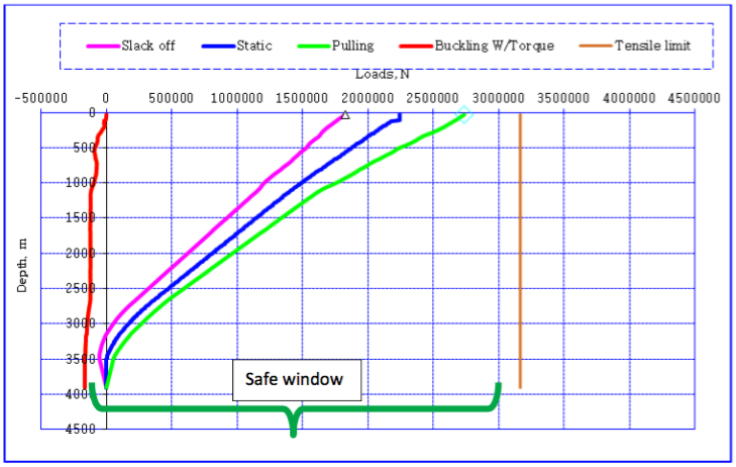

Figure 19: A safe drilling window is displayed between the two limiting forces; tensile and buckling limit. The friction forces are planned to be within the safe operational window Agonafir [2016].

1. Equilibrium condition: Newton's second law: Normal stress is given in Equation 24
2. Compatibility relation: Normal strain is given in Equation 25
3. Constitutive relation: Hooke's law is given in Equation 26

$$\sigma = \frac{F}{A_a} \tag{24}$$

$$\epsilon_s = \frac{\Delta L}{L_0} \tag{25}$$

$$\sigma = E\epsilon \tag{26}$$

$$\Delta L = \frac{FL_0}{EA_a} \tag{27}$$

$$\begin{aligned} \sigma &= \text{Normal stress} \\ F &= \text{Force} \\ A_a &= \text{Area} \\ \epsilon &= \text{Strain} \\ \Delta L &= \text{Change of length} \\ L_0 &= \text{Original length} \\ E &= \text{Young Modulus} \end{aligned}$$

Linking equations 24-26 together gives the load deformation in Equation 27.

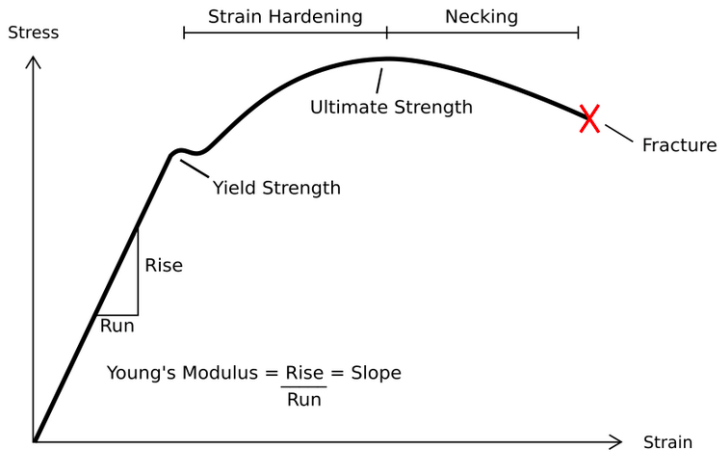

Figure 20: The tensile limit is determined by material test. A stress and strain diagram is the result of such a test. Yield strength value is used in calculation of tensile force Agonafir [2016].

The material the drill pipe is made of will have different properties that give different tensile limits. However, some metals are stronger, and have more resilience. These properties are detected in a stress and strain diagram, which is given in Figure 20.

To determine the tensile limit, some tests are performed to determine the parameters in Equation 28. The metal is applied a certain load, such that it is elongated. If more load is applied, the material will not go back to its original form. This is called permanent strain. When the material regains the same form after the load is taken of is called the elastic limit. The limit between the metal becomes plastic instead of elastic, and is associated with the term yield strength. Increasing the load from the yield point will lead to maximum stress before the material ruptures.

We differ between single loading and combined loading. Combined loading represents loading both axially and with applied torque. By principle stress failure criteria, one can relate the maximum principal stress with the yield stress in order to compute the axial stress. From axial stress we can determine maximum tensile load in Equation 29.

Of all metallic structures, fatigue is estimated to represent 90% of all failures. Stresses like axial, bending and torsional cause fatigue Agonafir [2016].

$$F_y = \frac{A_a \sigma_y}{SF} \tag{28}$$

$$F_a = A_a \left\{ \sigma_y + \frac{\tau^2}{\sigma_\theta - \sigma_y} \right\} \tag{29}$$

F_y = Tensile limit
F_a = Tensile limit, combined load
σ_y = Yield stress
SF = Safety factor
τ = Shear stress
σ_θ = Tangential stress

4.1.3 Buckling

The opposite of drag which creates tension is buckling, which is formed by compression of the drill string. Figure 21 states the difference between tension and compression. With increased force on the drill string, different orders of buckling will appear, in the first order sinusoidal buckling, applying more force will lead the drill string into the second order, which is helical buckling. Figure 22 and Figure 23 illustrate sinusoidal buckling and helical buckling in a wellbore. As you see, the sinusoidal shifts in 2D from right to left in a snaky manner, while helical would be compressed in 3D direction in a spiraling manner. Helical buckling will cause a great increase in the side force between the drill pipe and wellbore walls. The Dowson-Pasley's helical and sinusoidal buckling limits are represented in Equations 30 and 31. If buckling occurs it would result in increased well friction, the bit direction being off target, a stuck pipe situation, fatigue of the material, and the drill pipe losing stiffness and unable to provide weight on the bit Tveitdal [2011].

Buckling depends on $\rightarrow$ Stiffness of material + Outer diameter of the drill pipe compared to the wellbore/casing

$$F_{sin} = \sqrt{\frac{4EIwsin\alpha}{r}} \tag{30}$$

$$F_{hel} = \sqrt{2}F_{sin} \tag{31}$$

F_{sin} = Sinusoidal buckling
F_{hel} = Helical buckling
I = Moment of inertia
w = Weight per unit length
α = Angle of Inclination
r = Radius of drill pipe

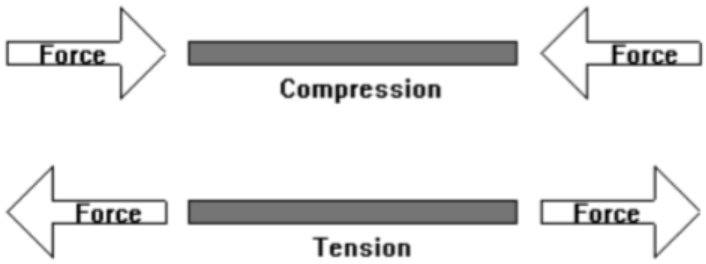

Figure 21: An illustration of compression and tension with forces applied Hendrix [2014].

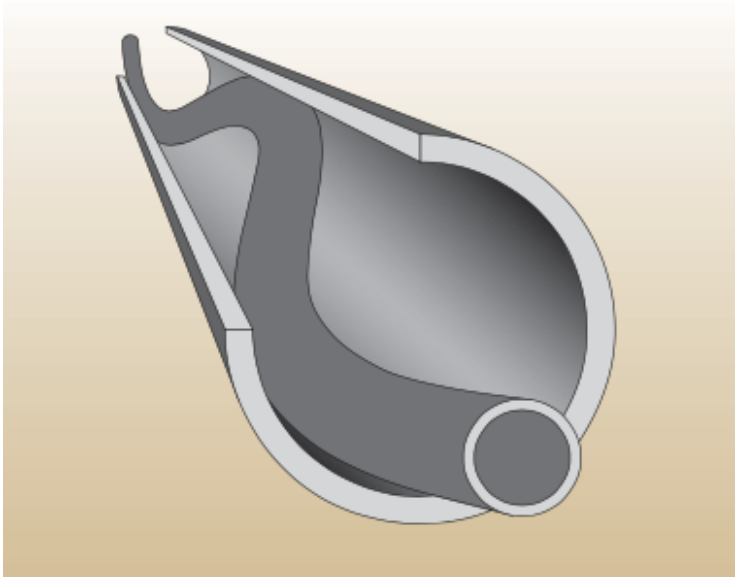

Figure 22: Sinusoidal Buckling. This is the first order of buckling when a load is applied Bennetzen et al. [2010].

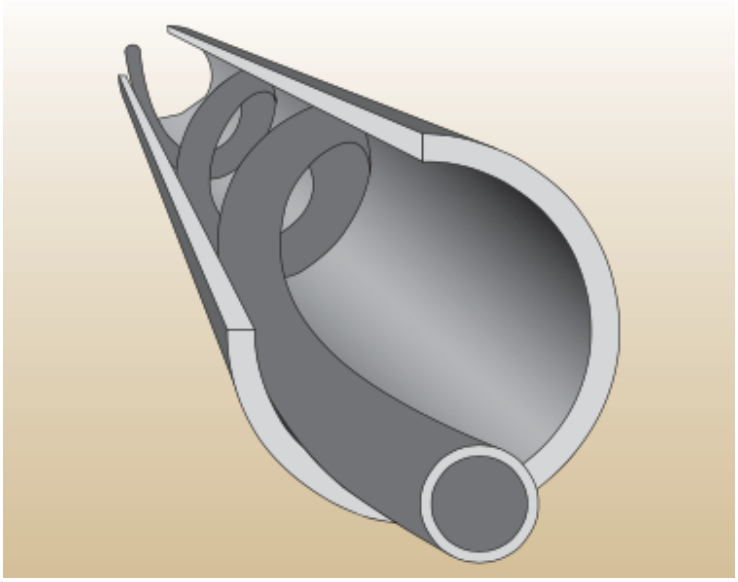

Figure 23: Helical Buckling. This is the second order of buckling when the load is applied, and the most critical Bennetzen et al. [2010].

4.2 Friction model

The friction forces that appear in the safe window between tensile and buckling limit in Figure 19 are introduced. The contact force between the wellbore and the drill string is determined to ensure the drill string won't failure during an well operation. The total force expected in the operation of rotating, pulling, lowering and keeping the drill string static in the wellbore is used in the well program of the well.

4.2.1 The soft-string model vs the stiff-string model

The soft-string model

The soft-string models that are used today are, in many ways, variations of Johancsik et al. [1984] studies. Instead of stiffness in the drill string material, we regard it as soft and that it rests on the wellbore as a cable, illustrated in Figure 25. Figure 24 displays the drill string, which is divided in multiple elements, the forces acting on each element is torsional and tension/compressive. Torque and drag is then summed up by adding each element from bottom to surface of the well. Contact forces are supported by the wellbore McCormick et al. [2011].

Johancsik et al. [1984] concluded that torque and drag are created by sliding forces in the system. The sliding force is a function of a normal contact force and the coefficient of friction (contact surface based on the Coulomb friction model). The soft-string model can, in many well situations, give a better indication of field data, but it ignores stiffness in material. For the model, this means that the bending moment effect and radial clearance is left out in the calculations Al-haj et al. [2015].

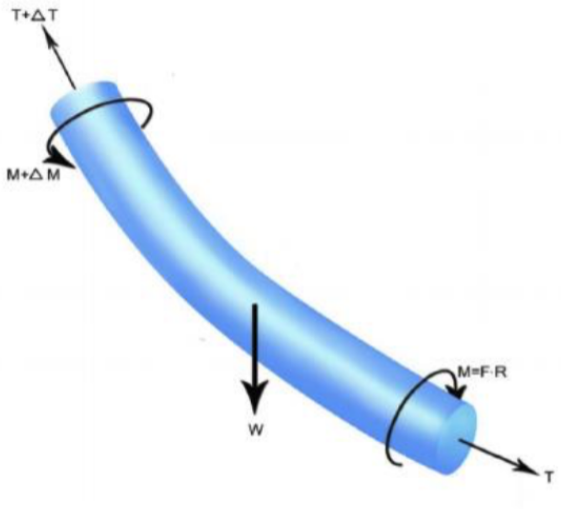

Figure 24: The drill string is divided into elements, and drag and torque calculations are performed on each element. The total force is the sum of all elements McCormick et al. [2011].

The stiff-string model

The stiff-string model differs from the soft-string model by implementing bending moment effects and radial clearance. The drill string is handled as a stiff material; therefore, it will not act as a cable along the wellbore as in the soft-string model. This is used to more accurately define torque and drag in difficult wells, such as extended reach wells. There has been improvement of this model since Johancsik et al. [1984] introduced it Al-haj et al. [2015].

Difference:

- The soft-string does not predict buckling onset
- The soft-string can underestimate drill string torque
- The soft-string model does not properly estimate contact side forces on the drill string
- The soft-string cannot monitor drill string mechanical integrity
- The striff-string model accounts for stiffness/bending and clearance/hole size

  "With these uncertainties, a risk of failure, lock-up drilling issues, casing wear, and poor overall drilling performance may appear. To properly estimate drill string loads, the stiff-string model with contact point calculation is highly recommended" DrillScan [2013]

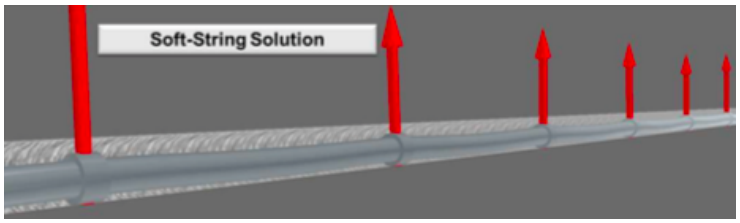

Figure 25: The soft-string solution act as a cable, neglecting the bending effects. The drill string is in contact through the wellbore DrillScan [2013].

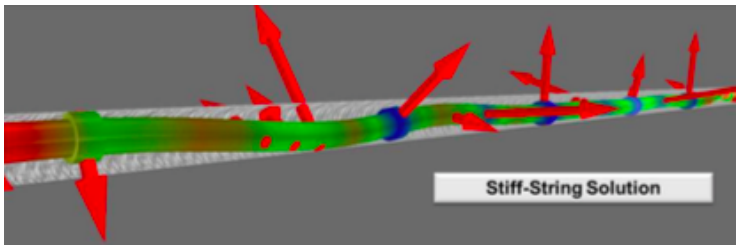

Figure 26: The bending effect is accounted for in stiff-string solutions, which is illustrated in the figure. The drill string has alternating contact with the wellbore DrillScan [2013].

4.2.2 Factors affect Torque and Drag

Torque and drag depend on parameters such as the friction factor, inclination, and length of the wellbore. Extended reach wells with steep deviations will cause high torque and drag forces.

Wellbore trajectory

Extended reach drilling is dependent on correct wellbore trajectory. The choice of wellbore trajectories give different torque readings. Torque needs to be decreased as much as possible. Therefore, we choose the well profile that gives the lowest torque readings from Table 18 and Figure 27. High angle wells will have more compression in the drill sting and less tension. This results in decreased torque in the system. Trajectory influences tortuosity, hole curvature, key seating, and dog leg severity. High tortuosity can severely limit the drillable length by resulting in high torque and drag; elimination of this effect is a critical factor. High tortuosity is caused by lack of control of toolface. Steerable motors are difficult to handle Al-haj et al. [2015].

Author	Contribution
Johancsik et al. (1984)	Introduced the soft-string model
Sheppard et al. (1987)	Made the soft-string model in a standard differential form. He also introduced mud pressure, which is the mud effect of running tubing in the wellbore. Effective tension = True tension + Mud pressure.
Maidla et al (1987)	By matching field data to the model, he back-calculated the friction factor that appeared in the well. He presented a method to evaluate overall friction.
Bret et al. (1989)	Were the first to plan a well by model before it was drilled. Used the model to identify drilling problems with analyzing previously-drilled wells. The information gathered made it possible to optimize wellbore trajectory, mud type, and casing setting depth to reduce torque and drag.
Ho (1988)	Implemented that the drill-collar stiffness effect is major over drill string and heavy weight drill pipe.
Opeyemi et al. (1998)	Well planning and drill-string design is, for the first time, determined by the torque and drag model.
Feiber et al. (1999)	Developed a computer model for torque and drag analyses. Friction factors are determined with matching of the hook load and torque.
Aadnoy and Andersen (2001)	Divided the well into different sections: build up, straight section and drop off. Introduced different equations to calculate the wellbore friction forces in these different sections.
Rae et al. (2005)	First to simulate torque and drag to plan a well.
Mason et al. (2007)	Improved the soft-string models by implementing factors, such as hydrodynamic viscous force, tortuosity effect, and crooked well profile vs smooth well profile.
Aadnoy (2008)	Created a 3D torque and drag model. Included side bend section from changes in azimuth.
Kaarstad et al. (2009)	Included studies of temperature in the wellbore into the 3D model. The friction factor is dependent on temperature. The result was introduced in the friction model.

Table 17: Displays the evolution of the stiff-string model Fazaelizadeh [2013].

Option	Advantages	Disadvantages
Multiple build profile: Rate of build increases with depth in several discrete steps to tangent angle, hold constant tangent angle	Very long reach, low torque/drag values, low casing wear	High tangent angle
Build and hold: Constant build rate to tangent angle, hold constant tangent angle	Simple, long reaches achievable, low tangent angle	Potentially high contact force in build (torque, casing wear)
Double build: Build-hold-build-hole trajectory, can use two different BURs in the build sections	Very long reaches possible with low contact forces in upper build	May require deep steering, high second tangent angle
Undersection: Build and hold with deep KOP	Reducing hanging weight below build section reduces contact force in build	High tangent angle, shorter reach
Inverted: Tangent angle above horizontal so the wellbore enters the reservoir from underneath	Flexibility for multiple targets, avoid gas cap	Higher axial (buckling) loads to push string uphill, deep steering required
3D: Any of the above with significant azimuth changes	Flexibility to handle anti-collision and multiple target requirements	More curvature means more torque and drag, deep steering may be required, shorter reach

Table 18: Displays description of different well profiles that is available to select in the planning phase of the well BP [1996].

Friction factor

Friction factor will thoroughly be introduced in Section 4.3. Friction is the main study of this thesis. Experimental work has been performed to research the modeled friction factor that is used in today's torque and drag model. The friction factor is the major constituent of torque and drag. Any reduction of friction factor will, therefore, give a direct reduction in torque and drag models.

Weight

Weight is a parameter that affects the calculation of normal force on the drill pipe. Lighter weight material will result in reduced drag and torque. A deal of effort is made to create a drill pipe that is lighter than today's selection, and is still able to give weight on bit, stiffness, and increased yield.

Mass of drill pipe, Equation 32, is found by density of the steel and the volume of the drill pipe. Steel is known to be used in extended reach wells, but

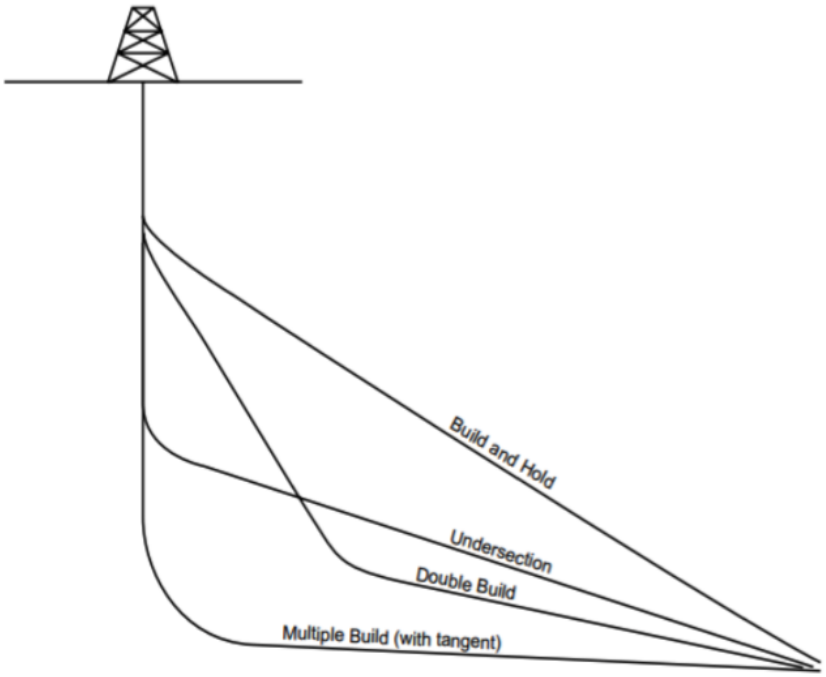

Figure 27: Illustrates the well profiles described in Table 18 BP [1996].

other materials, such as aluminum and titanium, which are lighter would give lower torque and drag. However, in many cases, these would not create enough weight on the bit.

Pipe weight is used to calculate the borehole normal force on the drill pipe in Equation 33. With the friction factor, we can find the friction force between the borehole and the drill pipe, as presented in Equation 34 Grindhaug [2012].

Weight is determined by → Material density + Pipe wall thickness

$$
\begin{aligned}
m &= \rho_s * V && (32)\\
F_n &= mgsin(\alpha) && (33)\\
F_f &= \mu F_n && (34)
\end{aligned}
$$

$$
\begin{aligned}
m &= \text{Mass}\\
F_n &= \text{Normal force}\\
F_f &= \text{Friction force}\\
\rho_s &= \text{Density steel}\\
V &= \text{Volume of steel material}\\
g &= \text{Gravitational constant}\\
\mu &= \text{Friction factor}
\end{aligned}
$$

Buoyancy

In Figure 28 the buoyant force acts in the opposite motion of gravity. The boat floats according to Archimedes' principle: The buoyant force on a submerged object is equal to the weight of the fluid that is displaced by the object. For drill pipes, the buoyancy equals the weight of the mud that the drill pipe displaces. Al-haj et al. [2015]. Equation 35 is relevant in a drilling operation where we assume the same drilling fluid in the drill pipe and the annulus. In cementing operations and displacement of mud, Equation 36, is used to calculate buoyancy. In such operations different fluids will occur in the drill pipe and annulus Grindhaug [2012].

$$\text{Buoyancy is determined by} \rightarrow \frac{\text{Suspended weight in mud}}{\text{Weight in air}}$$

$$
\begin{aligned}
\beta &= 1 - \frac{\rho_m}{\rho_s} && (35)\\
\beta &= 1 - \frac{\rho_{mo} r^2 - \rho_{mi} r^2}{\rho_{steel}(r_o^2 - r_i^2)} && (36)
\end{aligned}
$$

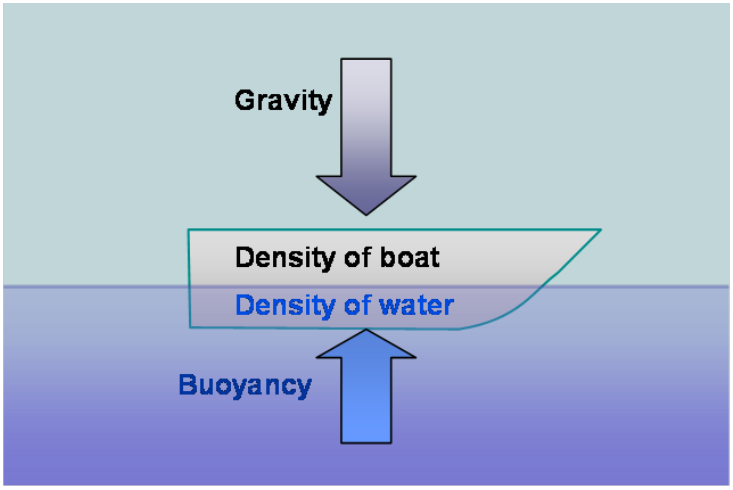

Figure 28: Illustration of buoyancy force that acts against the gravity and ensure floating off a boat Agonafir [2016].

$$
\begin{aligned}
\beta &= \text{Buoyancy factor} \\
\rho_m &= \text{Drilling fluid density} \\
\rho_{mo} &= \text{Drilling fluid density outside of the drill pipe} \\
\rho_{mi} &= \text{Drilling fluid density inside of the drill pipe} \\
r_o &= \text{Drill pipe radius outside} \\
r_i &= \text{Drill pipe radius inside}
\end{aligned}
$$

High mud density results in increased buoyancy factor. Increased buoyancy factor affects the torque and drag forces.

4.2.3 Drag

Drag is a force that appears when an object is moving and resistance appears in the opposite direction. An example in a drilling situation is when the drill sting is lowered/pulled in a tripping situation. It resists its motion to move by friction forces. The contact force seen in Figure 29 between the drill string and casing/formation, depending on closed/open hole, creates this drag by friction.

$$
\begin{aligned}
\text{Drag is determined by} &\rightarrow \text{Friction coefficient} + \text{Normal force exerted by the wall on the pipe} \\
\text{Normal force consists of} &\rightarrow \text{Drill string weight} + \text{Buoyancy} + \text{Well length} + \text{Inclination}
\end{aligned}
$$

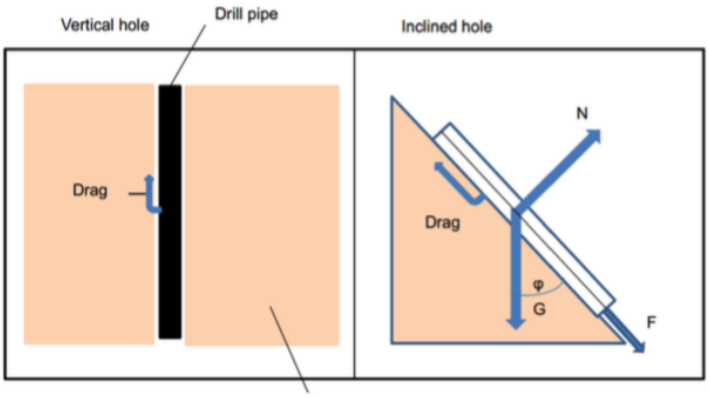

Figure 29: A lowering operation of the drill string where drag acts in the opposite motion in vertical and inclined holes . The contact force is the main difference Grindhaug [2012].

$$\text{Friction coefficient} \rightarrow \text{Axial friction (drill pipe and the wellbore)} + \text{Viscous friction (drill pipe and the drilling fluid)}$$

To be able to move the drill pipe, the top-drive needs to create forces to overcome the drag force. Total friction is created by many parameters and some parameters can be modeled, while others are taken care of with the friction factor.

Inclined model for drag

Drag force is normally not a problem in vertical wells, as the drill pipe hangs in the middle of the borehole, with less contact to create friction. In deviated wells, the drill pipe will rest on the wellbore and this increases the drag forces. Hole inclination is, therefore, an important parameter. Figure 29 illustrates the difference between a vertical well and a deviated wellu used in extended reach wells Al-haj et al. [2015].

Force balance equations, Figure 30:

$$\begin{aligned} Pulling \rightarrow \quad F &= mgcos(\alpha) + \mu mgsin(\alpha) && (37) \\ Lowering \rightarrow \quad F &= mgcos(\alpha) - \mu mgsin(\alpha) && (38) \end{aligned}$$

$$\begin{aligned} mg &= w\Delta s && (39) \\ w &= \beta w_{drillpipe} && (40) \\ w &= mg\beta = \frac{\pi}{4}(D^2 - d^2)\rho_s g(1 - \frac{\rho_m}{\rho_s}) && (41) \end{aligned}$$

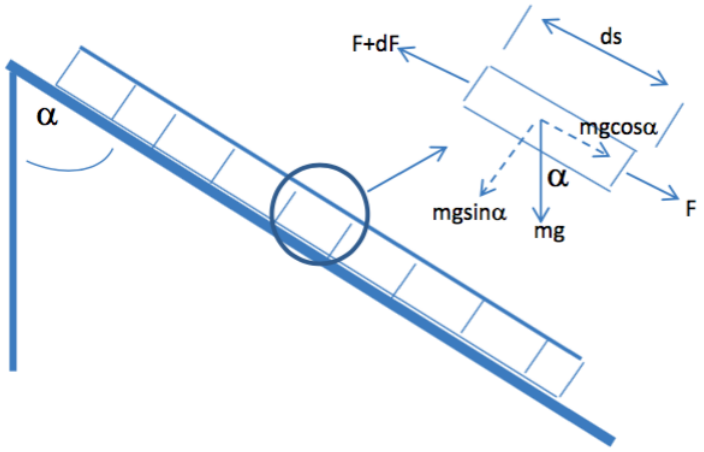

Figure 30: An illustration of the forces that appears on an element of drill pipe in an inclined well. The gravity, friction, and force from pulling or lowering act on the element. Friction factor is calculated from the normal force on the element Agonafir [2016].

$$\begin{aligned} \Delta s &= \text{Length of pipe} \\ D &= \text{Outer diameter, drill pipe} \\ d &= \text{Inner diameter, drill pipe} \end{aligned}$$

To be able to calculate the total drag in the system, we divide the wellbore into elements. By adding each element from the bottom of the well to the surface, we will get the total drag. Equation 37 refers to pulling of the drill string where friction and weight works against motion, and Equation 38 refers to lowering where weight would add on in the motion of the drill string and only friction works against the motion. We rewrite the static weight in Equation 39 and correct the weight for buoyancy with Equation 40. Equation 41 is a more detailed outline of the weight component.

From Figure 30, we derive equation 42 for weight and drag in a hold section of the well.

$$F_2 = F_1 + w\Delta s(cos(\alpha) \pm \mu sin(\alpha)) \tag{42}$$

The drag model applied in this study

The case studies made to illustrate the research performed in this thesis is carried out with the stiff-string model introduced by Aadnoy [2006]. Different types of models can be found in Table 17, each has different nuances in the calculation of

torque and drag, such as calculation of drag forces in the bend section, azimuth changes included, dog leg severity etc. A build and hold catenary well profile is selected in the case studies. Tables 19 - 21 calculates the drag force at the bit, on top of bottom hole assembly, at top of the sail section, at the kick-off position, and on top of well. The hook load modeled is the total force that appears in the different types of operation: such as static load, pulling, and lowering. The real-time hook load can be compared with the modeled hook load.

Force	**Equations, Static weight**
At Bit	$F_1 = 0$
Top BHA	$F_2 = F_1 + w_{BHA}L_{BHA}cos(\alpha)$
Top Sail section	$F_3 = F_2 + w_{DP}L_S cos(\alpha)$
At Kick-off position	$F_4 = F_3 + w_{DP}Rsin(\alpha)$
Top of well	$F_5 = F_4 + w_{DP}L_{KOP}$
Total	$F_{total} = \sum_i^{n=5} F_i$

Table 19: Static weight equations Aadnoy [2006].

Force	**Equations, Pulling**
At Bit	$F_1 = 0$
Top BHA	$F_2 = F_1 + w_{BHA}L_{BHA}(cos\alpha + \mu sin\alpha)$
Top Sail section	$F_3 = F_2 + w_{DP}L_S(cos\alpha + \mu sin\alpha)$
At Kick-off position	$F_4 = (F_3 + w_{DP}Rsin\alpha)e^{\mu\alpha}$
Top of well	$F_5 = F_4 + w_{DP}L_{KOP}$
Total	$F_{total} = \sum_i^{n=5} F_i$

Table 20: Pulling equations Aadnoy [2006].

Force	**Equations, Lowering**
At Bit	$F_1 = 0$
Top BHA	$F_2 = F_1 + w_{BHA}L_{BHA}(cos\alpha - \mu sin\alpha)$
Top Sail section	$F_3 = F_2 + w_{DP}L_S(cos\alpha - \mu sin\alpha)$
At Kick-off position	$F_4 = \left(F_3 + \frac{w_{DP}R}{1+\mu^2}((1-\mu^2)sin\alpha - 2\mu cos\alpha)\right)e^{-\mu\alpha} + \frac{2\mu w_{DP}R}{1+\mu^2}$
Top of well	$F_5 = F_4 + w_{DP}L_{KOP}$
Total	$F_{total} = \sum_i^{n=5} F_i$

Table 21: Lowering equations Aadnoy [2006].

4.2.4 Torque

Torque is the force needed to rotate an object about its axis. Tightening and loosening a bolt is an example of applying torque force. In drilling situations, torque is applied to the drill string to make it rotate. In a drilling scenario, normal force from friction multiplied by the distance to the outer diameter of the pipe causes the torque Mortensen and Brekke [2014].

Top-drive at the surface creates torque to the system that make the drill string rotate. Rotation of the drill string makes the drill bit rotate and crush formation. Long deviated wells and horizontals wells, such as extended reach drilling, have greater resistance to rotation because of excessive friction in the system. This implies more torque force must be added by top-drive to be able to overcome frictional forces. The limit of the rig and the drill string can hinder the drilling process. Extra torque to the system can lead to failure of the drill string by material yielding (make-up torque is exceeded, which is the drill string capacity) and top-drive must be able to handle surface torque that appears Grindhaug [2012].

$$\text{Surface torque} \rightarrow \text{Frictional torque} + \text{Dynamic torque} + \text{Bit torque}$$

$$\begin{aligned} \text{Frictional torque} &\rightarrow \text{Rotational friction against wellbore, contact friction} \\ \text{Dynamic torque} &\rightarrow \text{Viscous force between drillstring} \\ &\quad \text{and drilling fluid, fluid friction} \\ \text{Bit torque} &\rightarrow \text{WOB} * \text{Bit diameter} * \text{Bit aggressiveness} \end{aligned}$$

Dynamic torque is generated by cuttings bed, stabilizers effect, and liner centralizer.

The farther we drill, the more frictional torque will appear. Frictional torque is a function of the friction factor, side forces, axial load, and well profile. The parameters are illustrated in Figure 31, where the drill string is in contact with the wellbore while it rotates Al-haj et al. [2015].

$$\begin{aligned} \text{Torque is determined by} &\rightarrow \text{Radius of pipe} + \text{Friction coefficient} + \\ &\quad \text{Normal force exerted by the wall on the pipe} \end{aligned}$$

Inclined model for torque

Torque force is not a problem in vertical wells, as the drill pipe hangs in the middle of the borehole, assuming there is no contact with the wellbore to create friction. Torque generated by friction in inclined wells is represented in Equation 45: the buoyancy effect and angle of deviation is taken into consideration. This

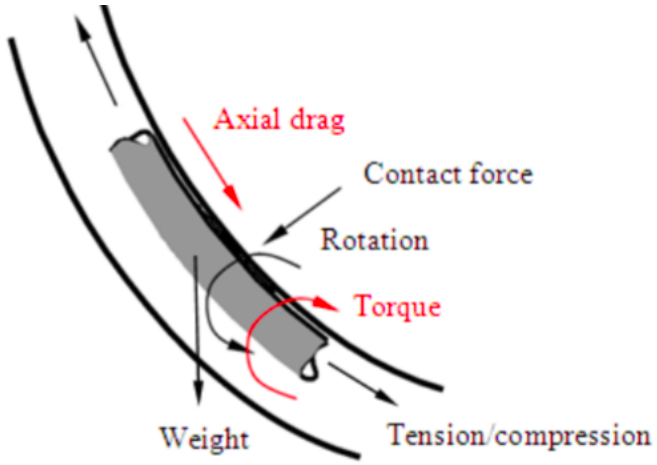

Figure 31: Illustrates the forces that appears on the drill string in a bend section. The drill string is in contact with the wellbore when rotating Wu et al. [2011].

is a simplified equation. Equation 44 is a more detailed equation, implementing the equation for weight component.

$$T_f = \mu waD \tag{43}$$

$$T_f = \mu \frac{\pi}{4} \left(D^2 - d^2\right) \rho_s gaD(1 - \frac{\rho_m}{\rho_s}) = \frac{D^2 + d^2}{4\sqrt{3}D^2 g(\rho_s - \rho_m)\mu} \tag{44}$$

$$T_f = \mu \left(w\Delta sr\right)(\beta) sin\alpha \tag{45}$$

$$\begin{aligned} T &= \text{Torque} \\ a &= \text{Horizontal length} \end{aligned}$$

The torque model applied in this study

As for drag equations, Aadnoy [2006] also introduced the formulas in Table 22 to calculate the torque force at bit, top of bottom hole assembly, at top sail, kick of point, and at top of well. As we can see from the equations, Aadnoy [2006] assumed no friction in the vertical section.

Force	Equations, Torque
At Bit	$T_1 = 0$
Top BHA	$T_2 = T_1 + \mu w_{BHA} L_{BHA} r sin\alpha$
Top Sail section	$T_3 = T_2 + \mu w_{DP} L_S r sin\alpha$
At Kick-off position	$T_4 = T_3 + \mu r * ((F_3 + w_{DP} R sin\alpha)\,\alpha + 2 w_{DP} R\,(1 - cos\alpha))$
Top of well	$T_5 = T_4$
Total	$T_{total} = \sum_i^{n=5} T_i$

Table 22: Torque equations Aadnoy [2006].

4.2.5 Torque and Drag reduction method

A summary of reduction measures is introduced in this subchapter. What is interesting to the reader is how we can reduce torque and drag forces that we have learned to know are severe in extended reach drilling wells. This thesis has its focus on friction factor and new ways of calculating the coefficient. However, as we see, there are many parameters that need to be optimized Al-haj et al. [2015].

- Wellpath
  - Tortuosity reduction by use of a rotary steerable system will make wellbores that are even.
  - Avoid high DLS in build up, drop off, and bends.
- Bit selection
  - Gauge length on drill bit affect the borehole outcome. With longer gauges on the bit, we avoid micro tortuosity that increases torque.
- Mud system
  - Oil-based mud is a better lubricator than syntethic-based mud and water-based mud, thus reducing friction in the system.
- Mechanical reduction techniques
  - Mechanical equipment, such as subs, is used to lift the drill pipe from being in contact with the wellbore. Subs are placed on each drill stand. They reduce contact friction and may be very effective in regard to extended reach drilling.

4.2.6 Basics of Torque and Drag modeling

We differ between modeling with known friction factor and unknown friction factor. The friction factor applied in the models can be given from the laboratory, this is called the modeled friction factor. The calculation can be done directly. When the friction factor is not known, we have to back calculate. The friction factor is measured from real-time torque and drag data. We iterate the model by assuming the friction factor until it matches real-time data. The drill string description and wellbore survey data are required Al-haj et al. [2015].

Torque and drag analysis have an essential part in drilling design. Benefits of torque and drag modeling:

- Trajectory design to minimize torque and drag forces.
- Assist in well planning and to predict and prevent drilling problems.
- To determine the drillability of the well and improve the design.
- To prepare the rotating system's rig capacity, the obtained surface torque data generated in the model could be a useful reference in determining the friction factor.
- To prevent buckling limitations when drilling the well, if the axial force tension or compression shown in the model exceed the critical buckling force, then the drilling plan must be readjusted.
- To prepare the rig capacity when the maximum hook load (including the safety factor and margin overpull) from the model is known.
- To know the magnitude of torque on the bit.
- To prepare the block weight and string configuration needed.
- An aid in determining if a change to the mud is necessary.
- Monitoring hole cleaning in real time.
- Determining if the drill string torque limits may be exceeded.

The list is given by Tveitdal [2011].

4.3 Tribology

Tribology is the science concerning friction behavior. Friction appears when two elements get in contact with each other and a drag will occur. There are two different types of friction; external and internal friction. External friction affects the surface of material. Internal friction affects the particles inside the material. We also separate between mechanical and dynamic friction, in drilling operation it is contact friction and fluid friction in the wellbore. In this thesis, mechanical friction will be the focus point. In drilling situations, mechanical friction appears between drill pipes and casing/formation Summers-Smith [1984]. Characteristics of material, such as abrasiveness and shape, determine the level of friction. Wear is proportional to friction, and is a complex matter that is dependent on parameters, such as material type, amount of friction applied, and type of movement between elements. Wear is defined as loss of material. When two metals are in contact with each other and friction appear between them, the hardness of the material defines which material scratches the other. The more friction, the more wear on the material, which can lead to fatigue Jahns [2014].

Friction forces are what causes torque and drag, so some basic theory on the subject will be presented in the following section. We divide friction into these options. Wikipedia-Friction [2016].

- Dry friction
- Fluid friction
- **Lubricated friction**
  - Fluid friction where a fluid divide two solid surfaces. Adequate fluid in between gives better lubrication and the result is equipment that last and only mild wear is applied. In drilling, drilling fluid act as the lubricator.
- Skin friction
- Internal friction

Friction is determined by inter surface adhesion, surface roughness, surface deformation, and surface contamination. These are complex parameters that need to be solved by empirical methods Wikipedia-Friction [2016].

The three frictional laws:

1. The force of friction is directly proportional to the applied load
2. The force of friction is independent of the apparent area of contact
3. Kinetic friction is independent of the velocity.

Author	Contribution
Aristotle (384-322 BC)	Aristotle was the first to recognize friction as a force against motion, and informed that friction was less for round objects.
Leonardo da Vinci (1452-1519)	Classic rules of sliding friction were discovered in da Vinci's unpublished notes.
Guillaume Amontons (1699-1705)	Amontons rediscovered friction and introduced surface irregularities and the force to overcome the weight of objects, which we call normal force. Amontons defined the first two laws of friction.
Leonhard Euler (1707-1783)	Euler contributed in Amontons study with objects on an inclined plane. He was the first to distinguish between static and kinetic force.
Charles-Augustin de Coulomb (1707-1783)	Coulomb studied the four main factors of friction: materials in contact and surface coating; surface area; normal force; and time of repose. Coulomb introduced the third law of friction.

Table 23: Displays the evolving history to the theory of friction **?**.

Coulomb friction model is used to calculate friction in systems, equation 46. It is an approximate model.

$$F_f = \mu F_n \tag{46}$$
$$F_n = mg \tag{47}$$

The Coulomb friction model may take any value from zero up to μF_n; the direction is against the applied force.

Normal and friction force

Normal force, F_n, is the component, which is perpendicular to the surface of contact. It supports the weight of the object. In a drilling situation the formation/casing supports the weight of the drill string in a wellbore. Normal force occur both in horizontal and inclined planes. Normal force can even be exerted horizontally between two objects. If a person leans on a wall, the wall will push back horizontally. This may transpire when a drill string is leaning on a vertical wellbore section.

The normal force illustrated in Figure 32 and stated in Equation 47, is parameters of mass and gravity affecting the object. The friction only appears when the object is moving in either direction. Pushing a box on a surface, such

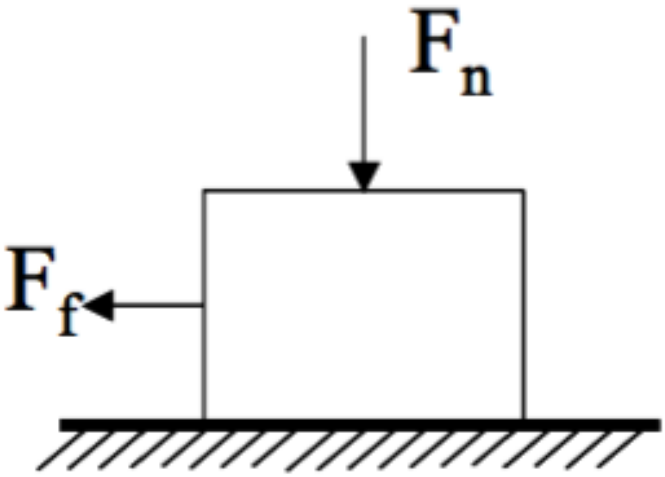

Figure 32: Illustrates the directions the normal and friction force act on a box on a horizontal plane when the box is in motion to the right Instruments [2010].

as ice, would be easier than if the surface was rock. Friction between the object and the surface will obstruct the movement. This is what we call friction force Wikipedia-Friction [2016].

Coefficient of friction

Antoine Parent introduced Equation 48; later, Euler found Equation 49, the angle of friction is defined as the angle on a inclined plane where static friction becomes kinetic friction (the object starts to slide). The coefficient of friction is a dimensionless scalar and is represented by the Greek letter, μ.

$$tan\theta = \frac{F_t}{F_n} \tag{48}$$

$$\mu = tan\theta \tag{49}$$

$$\theta = \text{Inclination of force}$$
$$F_t = \text{Tangential force}$$

The major parameter that affects the friction factor is the surface roughness. In drilling situations, this may relate to the surface of formation or inside the casing, and outside the drill pipe. The friction factor is dependent on these parameters Kaarstad et al. [2009].

- Humidity
- Surface roughness
- Viscosity
- Speed
- **Temperature**

Because of variables that occur during drilling operations, it is common to account for other effects that influence the friction factor Mason et al. [2007].

- Pipe stiffness effects
- Viscous drag, caused by pipe movement
- Cutting beds
- Lubricity loss, caused by loss of circulation
- Stabilizers/centralizers, affect string stiffness
- Tortuosity
- Hole cleaning
- Wellbore trajectory

The parameters are difficult to model because of their complexity. They vary over time, depth, and operation; such as pulling and lowering. The temperature effect on the friction factor is the main idea of this thesis, therefore the temperature will be thoroughly introduced in Section 4.4.

In a vertical well compared to a horizontal well, the friction factor has less affect on the torque and drag results. The drill string in a vertical well has less/negligible contact due to being placed more or less in the center of the borehole. Figure 33 seperated the well into a vertical section, bend section, and a horizontal hold section. The figure introduces the forces that appear in each section, and this profile is often associated with extended reach wells. The horizontal hold section is extended with great length and the drill string rests on the wellbore because of gravity effects. This results in contact friction. In the bend section, the drill string experiences both tension and compression alternating with rotation. The drill string is pushed against the top-side of the wellbore, which results in varying levels of torque and drag Mirhaj et al. [2011].

The friction factor is a critical factor in all operations, such as drilling, completion, workover and casing/liner hanger jobs Frafjord [2013].

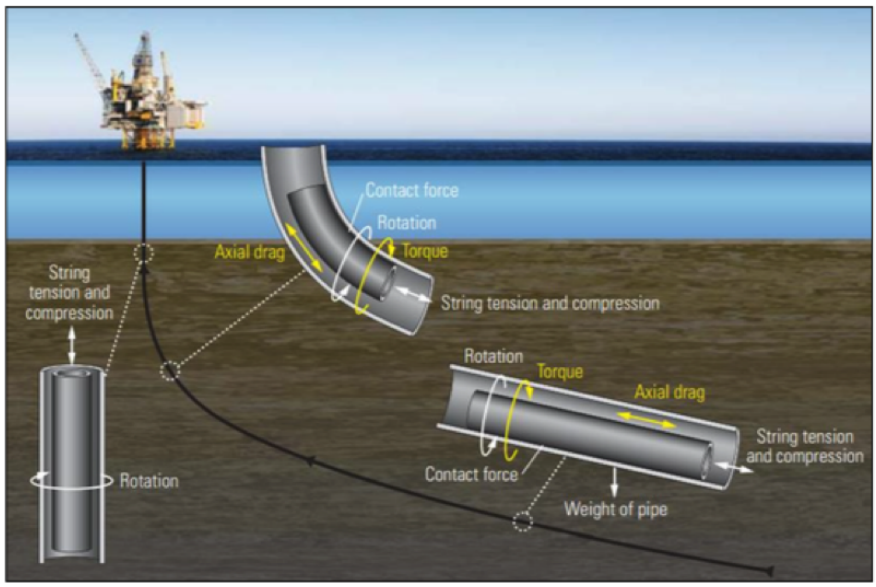

Figure 33: Illustrates forces on the drill string in deviated wellbore orientations. A vertical section, bend section and a hold section. As we can see there are different forces that acts in each section. The contact forces are negligible in vertical section in comparable to the hold section. The contact friction in bend section is towards the top-side of casing, where the drill string is alternating between compression and tension while rotating Bennetzen et al. [2010].

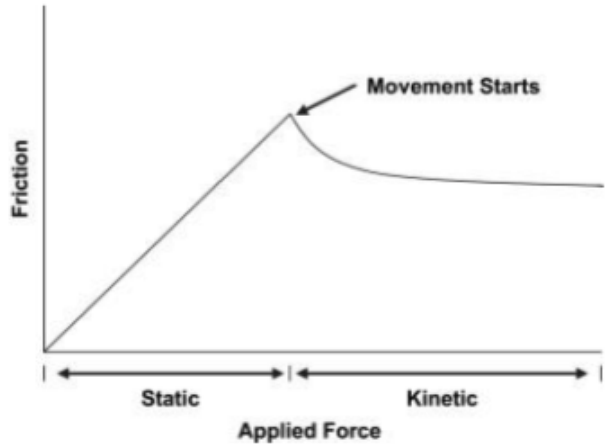

Figure 34: Shows two types of friction. Static friction is the friction the object experience when applied force, but the object is not in motion. Increase of applied force and the object starts moving. The friction that appears when the object is moving is called kinetic friction Burrow [2009].

Static and kinetic friction

Static friction is the friction that exists between two surfaces that are not moving relative to each other. Kinetic friction exist between two surfaces that are moving. During connection, installment of a new drill pipe on the drill string, the drill string is static in wellbore against the formation or casing. As soon as we start drilling, the drill string will move downwards and there will appear kinetic friction between the drill string and the formation or casing. We call this drag. Friction is either characterized as kinetic or static. In Figure 34 a typical behavior of static and kinetic friction is illustrated. A certain applied force is needed before an object starts moving, for example, pushing a heavy box. The friction is more when the object is static than when it moves. The force that is needed to push the box from a static posistion require more force than the force to push an moving box. Static friction is the force counteracting the applied force while kinetic friction is the force counteracting the pulling or pushing force Kaarstad et al. [2009].

Area of contact

Friction is proportional to the load and independent of the area of the sliding surface. A larger area of contact between two surfaces would create an increase source of frictional forces, it also reduces the pressure between the two surfaces for a given force holding them together. Int he relation in equation 50 it can be seen, that an increase in friction generating area, is exactly offset by the

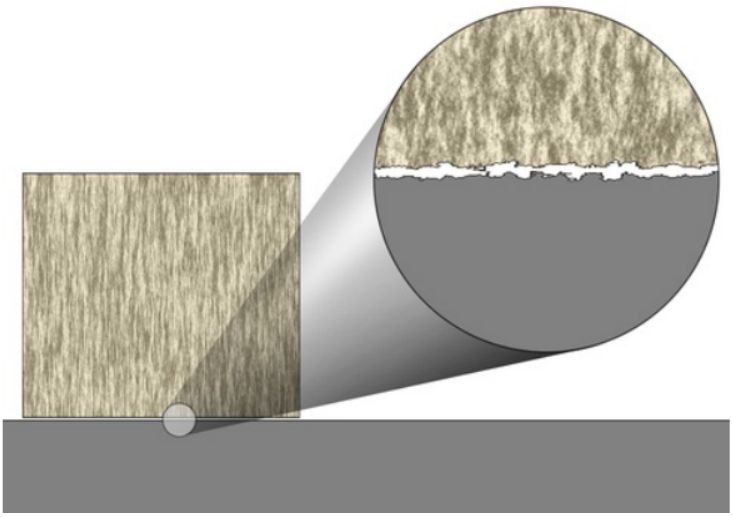

Figure 35: Illustrates the uneven surfaces between two objects. The real-area is dissimilar to the total-area regarding contact between two surfaces. However friction is independent of the area of the sliding surface Quoracdn [2016].

reduction in pressure. The frictional force is therefore dependent only on the frictional coefficient of the materials and the force holding them together. Increased force leads to increase of area to keep the pressure the same. Increase of area would increase the frictional force between the two surfaces. So even though the effective contact area is less than the total area, due to irregularities as seen in Figure 35 the friction won't be affected. Equation 51 indicates that the total area of contact is proportional to the normal force Kaarstad et al. [2009].

$$P = \frac{F}{A} \tag{50}$$

$$A_{total-areal} = const * F_n \tag{51}$$

P = Pressure

4.3.1 Wear mechanisms

There are different types of wear. They differ between:

- Abrasive wear
- Adhersive wear
- Fatigue

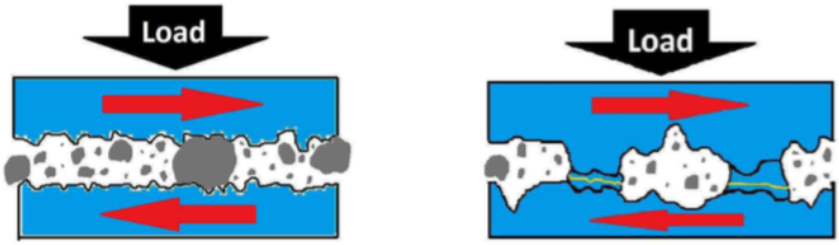

Figure 36: Load is applied pressing two surfaces together, abrasive wear occur of movement, while adhesive wear occur under high pressure. Left: Abrasive wear. Right: Adhesive wear Kjellevoll [2013].

- Corrosion

Abrasive wear is the most common in drilling situations. It is frictional movement where the harder element scratches the surface on the softer element. Volume and mass loss occur on the softer element. This wear is seen on the material sample in pin-on-disk apparatus and is the major wear that appears. Pin-on-disk apparatus is the experimental study done in this thesis and will be thoroughly introduced in Section 5. The wear is explained as machining, grinding, and polishing.

Adhesive wear happens when elements are under high pressure; this induces cold welding. Figure 36 gives an idea of how abrasive and adhesive wear differs.

Repeated impact of friction to the surface of a material may lead to fatigue. It will induce a crack and it will get deeper and deeper and eventually fail. Same as corrosion, fatigue happens over time. Corrosion is chemical reaction that affects the material. Corrosion is created by water, oil, and air conditions. When steel is in contact with water, the amount of ions in water will determine the corrosion rate of the steel. This become relevant in this study as water-based mud is used in experiments. There are different types of steel to choose from, some are better against corrosion than others, such as stainless steel. Corrosion changes the properties of the material by its effect on material surfaces Jahns [2014].

Equipment such as drill string, stabilizers, tool joints, crossover subs, and casing is exposed to wear. Drilling fluid between the borehole and the drill string will decrease friction. Eventually, the gap between the drill string and wellbore is narrowed, the drilling fluid becomes a thin film, which results in less effect of the lubrication from drilling fluid and increase in mechanical friction. Improvement of drilling fluid is done by adding additives like nanoparticles to increase the lubrication effect. Drilling fluid shall minimize the effect from all four wear mechanisms: abrasive, adhesive, fatigue, and corrosion wear Kjellevoll [2013].

Figure 37: The centralizers in red lifts the drill string from the wellbore. This results in less contact force Pvisoftware [2016].

4.3.2 Reducing friction

> "Torque and drag forces can be minimized by reducing the friction factor, and in so doing, increase the ability to drill farther and deeper wells." Aadnoy et al. [2010]

Devices

Equipment can be used to reduce friction. The sliding friction changes into a smaller sliding/rolling friction.

- Wheel
- Ball bearing
- Roller bearings
- Air cushion
- Fluid bearings

To reduce contact friction in wells because of excessive torque and drag forces, we use devices such as stabilizers and centralizers. On each drill pipe stand it is installed centralizers to lift the drill pipe from the wellbore. This results in less contact force. Figure 37 shows centralizers in red **?**.

Lubricants

Use of lubricants to reduce mechanical friction is quite effective. Oil, water, or grease is usually used as fluid between two solid surfaces. The science is called tribology.

Drilling fluid has many requirements to fulfill, one of them is to reduce friction. The composition of the drilling fluid defines the tribological behavior.

Parameters influencing tribological behavior:

- The size of the particles
  - Large particles are proportional to increased abrasive wear.
- The shape of the particles
  - Interaction with metal differs between sharp, rounded and spherical edges.
- The concentration of the particles
  - High concentration measures increased particle contact time towards the material surface.
- The particle solidify
  - Additive, such as nanoparticles, are supposed to act as ballbearings, but high forces overcome the solidness of these particles and the effect disappears.
- The forces acting on the material
- The material properties such as abrasiveness (asperity)
- The time frame of the material contact
- **The base fluid**

The major parameter that affects the drilling fluids' ability to act as a lubricant is the choice of base fluid. It can either be water-based mud, oil-based mud, or synthesized-based mud. Table 24 shows the difference in friction factor in open hole and cased hole when using different fluids. Oil-based mud is often used when drilling the deepest sections because of its qualities as a lubricator. The particles can move without attraction or repulsion because of non-polar properties of oil. Water-based mud is an ionic fluid and is naturally charged, which influences the lubrication property. Water is, therefore, naturally a less suitable lubricant, but it is environmental friendly. Top hole sections on the Norwegian continental shelf are by law, drilled with water-based mud. It is in everyone's interest to develop water-based mud so it can be used in the later sections in an extended reach drilling well Samuel [2010].

Drilling Fluid Type	Friction Factor	
	Cased Hole	**Open Hole**
Oil based	0.16 - 0.20	0.17 - 0.25
Water based	0.25 - 0.35	0.25 - 0.40
Brine	0.30 - 0.40	0.30 - 0.40
Polymer based	0.15 - 0.22	0.20 - 0.30
Synthetic based	0.12 - 0.18	0.15 - 0.25
Foam	0.30 - 0.40	0.35 - 0.55
Air	0.35 - 0.55	0.40 - 0.60

Table 24: Typical friction factor range is presented for different drilling fluid type Samuel [2010].

Nanofluids as additives could be the solution for water-based mud as it changes the rheological characteristics, decreases friction and mitigates wear. Friction decreases since the drilling fluid gets better as a lubricator because of surface energy changes by the absorption of nanoparticles and ball bearing effects (a smear film between the surfaces). Jahns [2014] researched the temperature effect on drilling fluids with nanofluid additives (titania and silica) with good results on reduced friction factors.

Author	Contribution
Ramsey (1962)	Introduced a heat transmission approximation regarding alternating hot and cold fluid.
Holmes (1969)	First analytical solution to temperature profile. The model gave good results, and assumed a steady state linear heat transfer.
Raymond (1970)	Claimed bottom hole fluid temperature varied with time and that it never achieved a steady state condition. Defined temperature profile as a function of motion convection, conduction from annulus/formation, and time. The model was solved numerically.
Keller (1973)	Developed a 2D model by employing finite difference equations. It included the effects of viscous flow energy, rotational energy, and drill bit energy. The equation was adaptable to casing and cement layers variations.
Thompson (1985)	Developed a computer model. They used a one-dimensional transient model and engaged the method of characteristics to solve it.
Kabir (1996)	Presented an easier analytical model for predicting temperature profile during normal and reversed circulation.

Table 25: Heat exchange literature review Apak.E.C [2006].

4.4 Temperature

The characteristics of drilling fluid have been developed over time with an aim to prevent degradation with temperature increase. For long, they only focused on improvement of the drilling fluid before they saw the significance of determining heat exchange to the wellbore. Table 25 displays the contributions in history of heat exchange.

Drilling fluid in the wellbore has different functions: clean the bit surface, transport cuttings, provide hydrostatic pressure against formation pressure, and act as lubrication to minimize friction. The drilling fluid gets heated in the wellbore by warmth of formation. This may change characteristics in the drilling fluid, such as rheology and density. Torque and drag can become a severe problem, as the friction factor increases with the temperature, and the result may lead to failure of the drill string. Temperature effects is therefore important to implement in planning of a well.

We differ between circulating and static drilling fluid in well. Even though

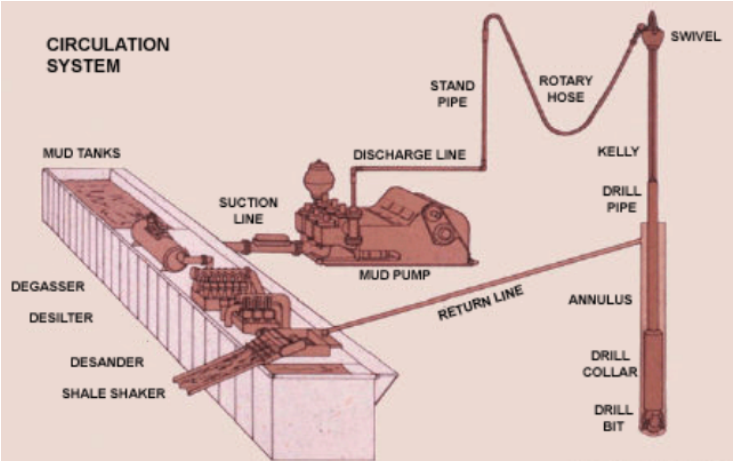

Figure 38: Displays the mud circulation system on a drilling rig. Circulated mud is pumped through stand pipe and rotary hose, into the drill pipe, through the drill bit where it returns back in annulus, and return line. The mud is returned with formation cuttings, and is therefore decontaminated in the shaker and desander. Any gasses that is contained in the mud are separated in the degasser before it returns back into mud tanks and are ready for re-use LABOR [2016].

static fluid in the well would provide enough hydrostatic pressure, we need circulating mud to transport cuttings and clean the bit surface. Illustrated in Figure 38, mud is circulated through a drilling fluid tanker, sent down into the drill pipe, through drill bit, back up through annulus, and to surface where it is decontaminated before it goes back into the drilling fluid tanker where it is ready be re-used Apak.E.C [2006].

When drilling fluid in the annulus gets heated by formation, the drilling fluid in the annulus will heat the drilling fluid in the drill pipe. It is important to determine both temperatures and control them. Too much heated drilling fluid, could create problems such as flocculation and disperson. We use additives to minimize the effect.

- Flocculation
  - Gel strength of the fluid dramatically increases and wool-like structures. Increasing the shear rate of the fluid Annis et al. [1967].
- Dispersion
  - As the exposure time to high temperatures increases, so does the number of individual platelets in suspension because of dispersion of clay minerals. This would permanently increase the viscosity Browning et al. [1963].

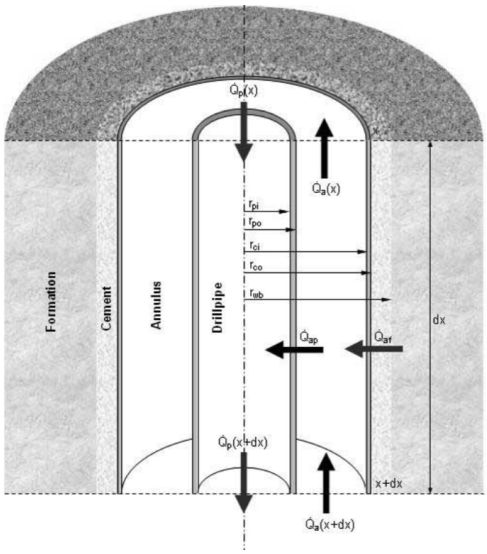

Figure 39: The formation, cement, annulus and drill pipe steel acts as thermal resistance in wellbore Apak.E.C [2006].

The temperature increases as the depth increases because of geothermal gradient of the earth. As wells get deeper, the temperature of drilling fluid slowly rises until degradation occurs and drilling fluid becomes solid.

Figure 39 illustrates the thermal resistance that occurs in a wellbore, such as drill pipe, casing, and cement layers. This thermal ressistance is accounted for in the models, which calculates the drilling fluid temperature. A temperature profile in a fluid flowing well is necessary. The physical and chemical properties changes as the drilling fluid is heated. A temperature model is used to avoid problems. by predicting the temperature in wellbore so it can be controlled Apak.E.C [2006].

4.4.1 Geothermal gradient

A geothermal gradient implies the rate of increasing temperature with depth in to the earths interior. At the center of the earth, the temperature is approximately 7000 kelvin. At a depth of 3500 km, the temperature is estimated to be 5650 ± 600 kelvin. This would be at the boundary of the outer and inner core, white and grey in Figure 40. The heat comes from a combination of residual heat from planetary accretion, heat produced through radioactive decay, and heat from other sources. The mantle is created by high density with many small radii atomic atoms. The heat is stopped by the earth crust, which works as an insulating blanket together with the lithosphere and plate tectonics. The heat from the earth can be used as an energy source- this is called geothermal energy.

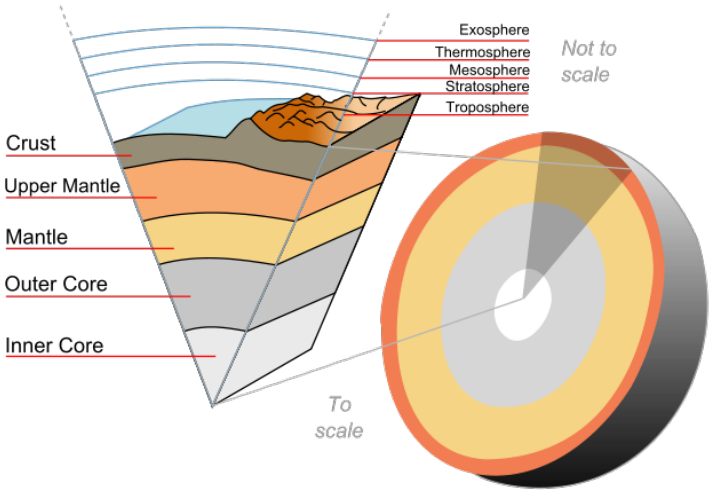

Figure 40: Earth layer illustration Wikipedia[2016].

To be able to determine the formation temperature in a drilling operation, we need to set a geothermal gradient. The geothermal gradient varies depending on the geographical location. Fouries law of heat applied to the earth gives local geothermal gradient. Geothermal gradient is actually measured by determining the bottom open hole temperature after drilling the well. The drilling fluid must be static and reach ambient temperature. The global average is 20 K/km or more in deep boreholes. Changes in surface temperature caused by the climate can affect the geothermal gradient Wikipedia-Geothermal [2016].

4.4.2 Temperature model of Apak

Assumptions

Temperature in a wellbore is affected by:

1. Frictional energy losses due to the drill pipe contacting casing or borehole during rotation
2. Viscous energy losses of the drilling fluid
3. Energy loss of the cuttings
4. Frictional energy losses from the bit
5. Heat flow from the formation

The major effect arises from heat flow from the formation and is assumed to be the only heat source in Apak.E.C [2006] solution. The assumptions is made by Apak.E.C [2006] in the following list:

- The problem is reduced to one dimension by assuming no heat conduction in the axial direction. The heat is conducted only radially to the wellbore.
- Heat flow in the wellbore is assumed to be steady state and heat flow in the formation is assumed to be transient.
- Viscosity and density of the flowing fluid is assumed to be constant with respect to changing temperature, and fluid is assumed to be incompressible. This assumption does not have a big impact on the solution.
- Fluid is assumed to be at a constant temperature across the cross sections of the drill pipe and annulus; thus, axial temperature distribution is a straight line.
- Heat flow from the formation is assumed to be only conduction and approximated by an equation that utilizes Fourier's dimensionless temperature function.
- Temperature of the fluid at the end of the drill pipe is assumed to be the same as temperature of the fluid entering the annulus.

Temperature calculation

Table 26 illustrate the formulas to calculate the coefficients used in equations 52-56 to calculate the temperature distribution in the drill pipe and annulus. A simple empirical correlation, equation 54-56, to predict the temperature profile of the drill pipe, annulus, and max temperature in the wellbore is derived.

> "An analytical solution for estimating the temperature of a fluid flowing through a drill pipe and annulus as a function of depth and time." Apak.E.C [2006]

Many variables acquire many assumptions. Variables to the solution that had significant effect are depth, flow rate, time, geothermal gradient, formation specific heat, formation conductivity, fluid inlet temperature and surface earth temperature. Variables, such as pipe and annulus diameter, formation density, fluid density, viscosity, formation specific heat and conductivity has negligible effect to the solution of drilling fluid temperature Apak.E.C [2006].

Temperature distribution in the drill pipe:

$$T_p = C_1 e^{\theta_1 x} + C_2 e^{\theta_2 x} + Gx + T_s - \frac{G}{A} \tag{52}$$

Temperature distribution in annulus:

$$T_a = \left(1 + \frac{\theta_1}{A}\right) C_1 e^{\theta_1 x} + \left(1 + \frac{\theta_1}{A}\right) C_2 e^{\theta_2 x} + Gx + T_s \tag{53}$$

Empirical correlation:

Type	Equation
Cross-sectional area, drill string and annulus	$A_p = \pi r_{o-dp}^2$
	$A_a = \pi(r_{bit}^2 - r_{o-dp}^2)$
Reynolds number: drill string, annulus and prandtl number	$N_{rep} = \frac{\mu_{mud} C_f}{K_f}$
	$N_{rea} = 0.816 \frac{2(r_{bit} - r_{o-dp})m}{A_a \mu_{mud}}$
	$N_{pr} = \frac{\mu_{mud} C_f}{K_f}$
Heat transfer of drilling fluid, drill string and annulus	$h_p = 0.023(N_{rep})^{0.8}(N_{pr})^{0.4} \frac{K_f}{2r_{o-dp}}$
	$h_a = 0.023(N_{rep})^{0.8}(N_{pr})^{0.4} \frac{K_f}{2r_{bit}}$
Overall heat transfer of drilling fluid in drillstring	$U_p = (\frac{1}{h_p} + \frac{r_{i-dp}}{K_p} ln \frac{r_{o-dp}}{r_{i-dp}} + \frac{r_{o-dp}}{r_{i-dp} h_a})^{-1}$
	$U_a = h_a$
Heat diffusivity of formation	$\alpha = \frac{K_f}{c_f \rho_f}$
Dimensionless temperature	$t_{D=} \frac{\alpha t}{r_{bit}^2}$
	$T_D = (0.4063 + 0.5 ln(t_d)) * (1 + \frac{0.6}{t_d})$
Model coefficient	$A = \frac{2\pi r_{o-dp} U_p}{\rho_{mud} m C_f}$
Model coefficient	$B = \frac{2\pi r_{ci} U_a K}{(\rho_{mud} m C_f) * (K + r_{ci} U_a T_D)}$
Model coefficient	$\theta_1 = \frac{B + \sqrt{B^2 + 4AB}}{2}$
Model coefficient	$\theta_2 = \frac{B - \sqrt{B^2 + 4AB}}{2}$
Model coefficient	$C_1 = \frac{-(T_{pi} - T_s + \frac{G_s}{A}) \theta_2 e^{\theta_2 H} - G_s}{(\theta_1 e^{\theta_1 H} - \theta_2 e^{\theta_2 H})}$
Model coefficient	$C_2 = \frac{(T_{pi} - T_s + \frac{G_s}{A}) \theta_1 e^{\theta_1 H} + G}{(\theta_1 e^{\theta_1 H} - \theta_2 e^{\theta_2 H})}$

Table 26: Introduces the formulas to calculate the temperature of drilling fluid at desired depth. The coefficients discovered are used in the temperature Equations 52-56 Apak.E.C [2006].

$$T_p = T_{pi} - 0.3207t + 0.0465x + 1193.65G - 0.0166q - 1.0401T_s \tag{54}$$

$$T_a = T_p - 0.00945t + 0.000006x + 47.869G - 0.00387q - 0.05112T_s \tag{55}$$

$$T_{max} = 0.7238\,(t)^{-0.0488}\,(x)^{0.8153}\,(G)^{0.7279}\,(q)^{-0.0879}\,(T_{pi})^{0.0857}\,(T_s)^{0.3622} \tag{56}$$

$$\begin{aligned}
T_p &= \text{Fluid temperature in the drill pipe} \\
T_a &= \text{Fluid temperature in annulus} \\
T_{max} &= \text{Maximum fluid temperature in the well} \\
\theta_1, \theta_2, \alpha, \beta, C_1, C_2, A &= \text{Constants} \\
x &= \text{Depth of interesting target} \\
G &= \text{Geothermal gradient} \\
T_s &= \text{Surface earth temperature} \\
T_{pi} &= \text{Inlet drill pipe temperature} \\
t &= \text{Circulation time} \\
q &= \text{Volumetric flow rate} \\
H &= \text{Depth of well}
\end{aligned}$$

Analytical Solution

In the analytical solution of Apak.E.C [2006], a different set of parameters is tested. The geothermal gradient is set to 3.65 F/100ft. This geothermal gradient is above average global geothermal gradient.

The profile is tested with different set of parameters:

- Change of temperature profile with different flow rates, inlet temperature, formation specific heat, surface earth temperature.
- Change of maximum temperature with pump rate.
- Change of temperature profile with different circulation time.
- Change of maximum temperature with different circulation time.
- Change of temperature distribution in a well with different number casing strings.
- Temperature distribution in a 5000 ft well.

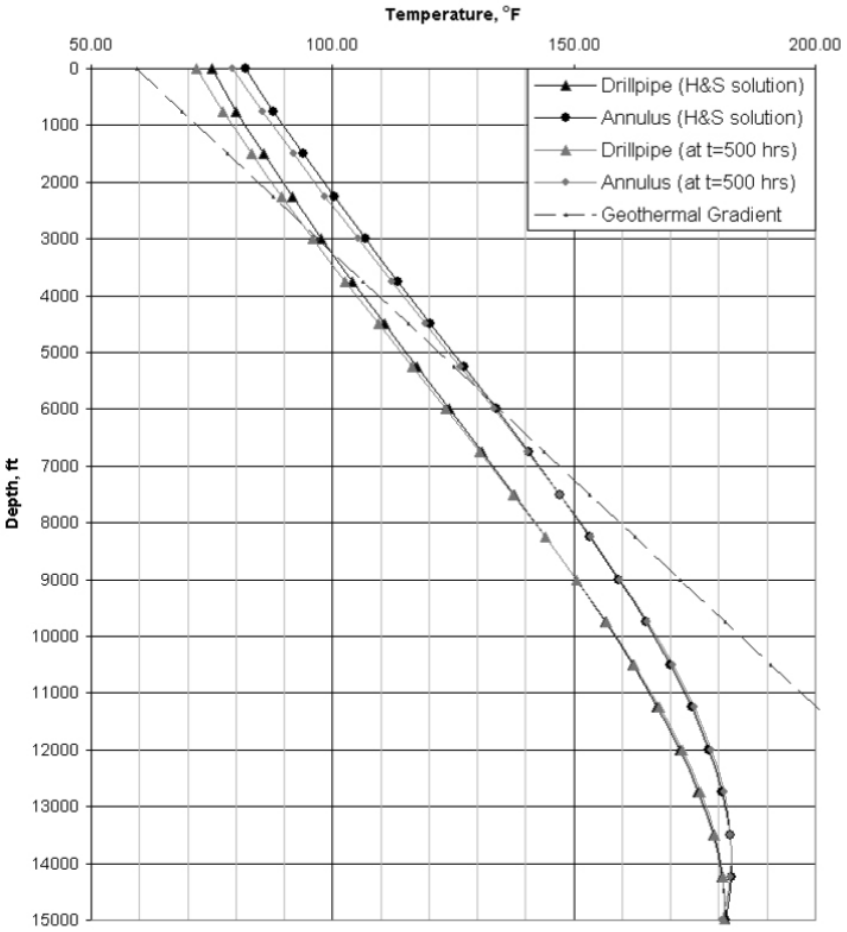

Figure 41: Temperature profile of geothermal gradient, Apak, and Holmes and Swift. The temperature model improves the accuracy of calculating the drilling fluid temperature in the wellbore at increased depth Apak.E.C [2006].

The result of parameter testing gave indications that the temperature profile is dependent on circulation rate and circulation time. Either the formation heats the drilling fluid or the drilling fluid cools down the formation. With high circulation, formation cool down will occur and the fluid won't be heated as a more static fluid would. Number of casing strings, thermal properties of the formation, and the inlet temperature will have little effect on the temperature profile, especially on maximum temperature were no significant change was seen. The well profile is only accurate of wells deeper than 5000 ft. The maximum temperature is accurate enough to be used in a field operation with 6,7% average error.

5 Experimental friction measurements

Tribology can be studied by different lab equipment. Pin-on-disk is used in this research to measure friction factor and the lubricity effect of the drilling fluid. To be able to compare the different equipment, there is an international standard for measurement. G99-05 [2010] is the standard for pin-on-disk. The testing procedure is affected by laboratory conditions and the existing instruments. It is, therefore, difficult to set a standard and the testing procedure has to be individually adjusted. Tribology includes different lubrication stages:

- Thin film lubrication
- Boundary lubrication
- Mixed lubrication
- Hydrodynamic lubrication

These stages are only visible in the laboratory and not to the naked eye. The parameters that affect the lubrication stages are different in the laboratory, than in a real well operation. Thin film and boundary lubrication are vulnerable to humidity, vibrations, and environmental sounds that exist in a laboratory Summers-Smith [1984].

For comparison of tests, the exam procedure should be executed in a consistent manner. G99-05 [2010] describes, in detail, the procedure to follow. It defines:

- Orientation
- Alignment of equipment
- Execution of test
- Presentation of results

Figure 42: Displays the tribometer used in the experiments to solve the main idea of this thesis. Determination of local friction factor in wellbore Instruments [2010].

5.1 Pin-on-disk equipment

The tribological measurement instrument is provided by the tribology lab of the University of Stavanger.

The pin-on-disk apparatus in Figure 42 has a one sided open cylinder which we call the disk. The material sample is installed in a fixed position with three screws and, since we are performing the test with a fluid, a sample holder is installed. The friction test can be performed either in rotation or linear motion.

There are different types of pin-on-disk equipment, but all of them have the same principle. A cylindrical pin with an installed ball at the end of it is pushed towards the material sample with a selected load. We set a rotational diameter. According to this rotational diameter, the sliding speed and sliding distance can be adjusted. Some pin-on-disk equipment allows for temperature modification on drilling fluid. A heating spiral is installed in the sample holder. All types of fluid can be used in this experiment. Figure 43 is an illustration of the pin-on-disk measurement principle.

Other than friction, wear can be measured by calculating the volume loss either on the pin or the material sample. By ASTM standard it is possible to determine the wear which appears after experiment is performed by measuring

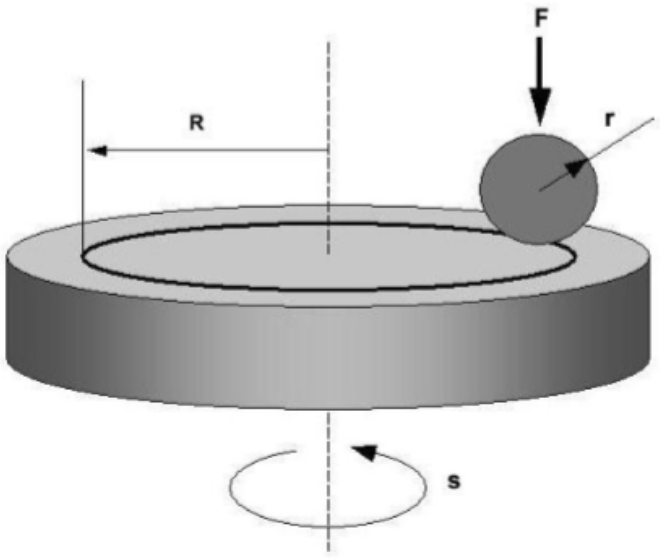

Figure 43: Typical ball-on-disk setup where F is the normal force applied on the ball, r is the ball diameter, R is the radius of the wear track and s is the rotational speed of the disk Instruments [2010].

linear dimension of both materials or weighing before and after the test. The rotational friction motion simulates a drill string in casing. Different settings can be selected such as; the normal force applied on the ball, the radius of the ball, the wear track and, the rotational speed. Wear can occur in three options between the ball and material sample, the ball is the soft material, the sample is the soft material, the ball and material is equally hard. The options is shown in Figure 44. Instruments [2010]

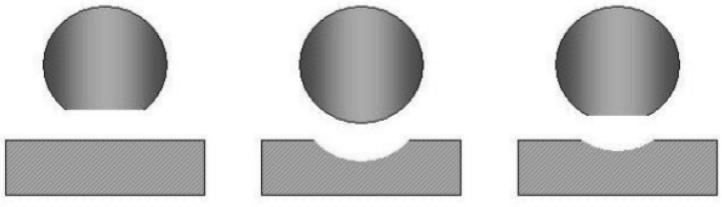

Figure 44: Wear resistance of ball and sample Instruments [2010].

5.2 Fluid composition

Mi-Swaco accepted our request of testing their drilling fluid. Quality drilling fluid is a caterpillar to achieve good results on the experiment, this was provided by MI-Swaco. Table 27 introduces the additives MI-Swaco can implement into drilling fluid to address all downhole problems.

> "Our custom-formulated fluid systems and additives help operators enhance drilling efficiency while decreasing costs and mitigating HSE impact. With a suite of filtercake breakers, corrosion inhibitors, shale inhibitors, and much more, M-I SWACO has the extensive portfolio of advanced solutions and in-depth expertise to help you meet your operational goals—no matter the job's challenge, location, or size." MI-Swaco

> "MI-Swaco offers a range of chemical products formulated to reduce the coefficient of friction , helping you minimize torque and drag, reduce stuck pipe risk, and increase ROP." MI-Swaco

An example of manually mixing of water-based drilling fluid:

1. Mix water with bentonite, ensure complete hydration of the bentonite by letting it rest for 30 minutes.
2. Add polymers and mix in the brine.
3. Use density measurement to calculate the amount of barite to add.
4. To ensure well dispersed fluid components, the mixing is done for at least five minutes.
5. Nanoparticles are added at the last stage.

To be able to do comparable samples it is an advantage to keep it simple, with no further variation and additional components, and use it in the same day as it eliminates the aging process as a possible error source. The mud is ready to get heated and tested as a lubricator illustrated in Figure 47 Jahns [2014].

Additives	Function
Alkalinity control	Adjust and regulate the degree of acidity or alkalinity of drilling fluids.
Bactericides	Prevent bacterial degradation and reduce the souring of drilling mud.
Corrosion inhibitors	Mitigate corrosion, neutralize hazardous acid gas, and prevent the formation of production-impairing scale.
Defoamers	Counteract the formation of foam, which can negatively impact the production process as a result of liquid carryover.
Emulsifiers and wetting agent	Control filtration and stabilize temperatures.
Filtration reducers	Reduce formation fluid loss caused by the liquid phase of the drilling fluid.
Flocculants	Increase the viscosity of water-base drilling fluids to enhance hole cleaning.
Foaming agents	Improve air or gas drilling through water-bearing formations with chemical offerings that serve as surfactants.
Lost circulation materials	Improve air or gas drilling through water-bearing formations with chemical offerings that serve as surfactants.
Lubricants	Reduce the coefficient of friction to minimize torque and drag while drilling with water-base fluid.
Pipe-free agents	Free pipe with spotting or soaking agents for all types of drilling fluids.
Scale inhibitors	Inhibit the deposition of mineral scales.
Scavengers	Drill effectively with scavengers that are effective at the pH levels found in most drilling fluids.
Shale inhibitors	Inhibit reactive shales with a suite of low-toxicity, environmentally acceptable additives
Surfactants	Reduce interfacial tension between water/oil, water/solid, water/air, and other contacting surfaces.
Temperature stabilizers	Increase the rheological and filtration stability of drilling fluids, and improve the thermal stability in higher-temperature environments.
Thinners and dispersants	Help modify the relationship between the viscosity and percentage of solids in drilling fluids.
Tracers	Maximize contact with formation waters to improve water-sampling performance.
Viscosifiers	Improve the hole-cleaning and solids-suspension capability of drilling fluids.
Weighting agents	Control formation pressures, prevent formation caving, and facilitate the pulling of dry pipe.
Wellbore strengthening materials	Strengthen unstable wellbores, minimize lost circulation, and mitigate other issues that can jeopardize project efficiency and economics.

Table 27: Additives and their function is presented. Quoted from Schlumberger website.

5.3 Method of experimental testing

The method used to get comparable results in the experiment is listed below.

1. All surface components and small-scale particles must be removed before starting the experiment. It is recommended to use ethanol in the cleaning process. Either use air pressure to remove remaining water or let it dry up. Figures 45-47 displays where different components are placed in the tribometer.

   (a) Disk
   (b) Screws
   (c) Sample holder
   (d) Material sample
   (e) Pin with the steel ball
   (f) Heating spiral
   (g) Thermometer

2. The material sample is screwed in place in a fixed position in the middle of the sample holder. The material sample can be of different types of steel and rock. In this study, it is used a typical casing steel: ST57. The dimension of the sample is 2.5 x 2.5 x 0.5 to be able to fit in its place. The ball placed in the cylindrical pin is stainless steel AISI 316 of grade 100 with 6 mm diameter.The hardness of stainless steel ensures that the wear occurs on the material sample. The ball is tightened in the pin.

3. The heating spiral is placed in the sample holder, as close as possible to the bottom without being in contact with other components. This component is connected to the computer program so that we can specify the temperature wanted.

4. The pin holder arm requires calibration to a horizontal level; this eliminates inclinations that could affect the result by manipulating the load applied. The pin holder arm is elevated until the experiment starts. See Figure 47 for an illustration.

5. Fluid is added into a sample holder. It should cover the heating spiral and account for loss of fluid because of heating. Approximately 150 ml. Figure 46 exemplify drilling fluid to cover the heating element.

6. The preferred load is put on top of the pin when the fluid has reached the preferred temperature. An example of 10 newton is applied in Figure 47.

The experiment is observed on a computer. It allows for different settings, such as humidity and temperature in the laboratory, sliding speed, and sliding distance. In this research, we will study the effect temperature has on the friction coefficient. The temperature of the fluid is increased from 30 degrees to 70

degrees with intervals of 10 degrees. In the preheating phase, the sample holder is in constant rotation mode as it ensures constant temperature distribution and the fluid is in constant motion. When temperature has reached a desired temperature, the arm of the pin holder is set in contact with the material sample and a load of 10 newton is applied on the top of the pin. At each step, the load is consistent. The experiment shall be completed without disturbance, such as noise, jamming and interruption. If disturbance occurs the test result may be degraded.

The material sample can, after the experiment, be examined for wear calculations. But this is not pursued in this research.

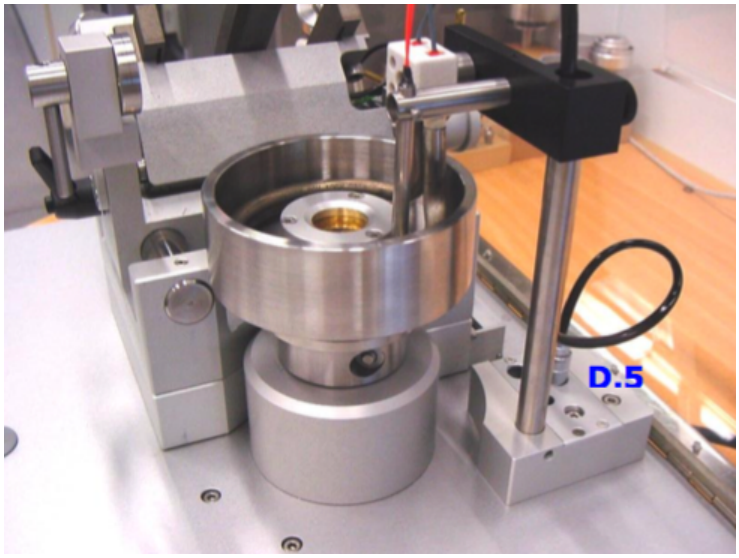

Figure 45: The material sample is screwed in place inside of sample holder. The heating element is installed Instruments [2010].

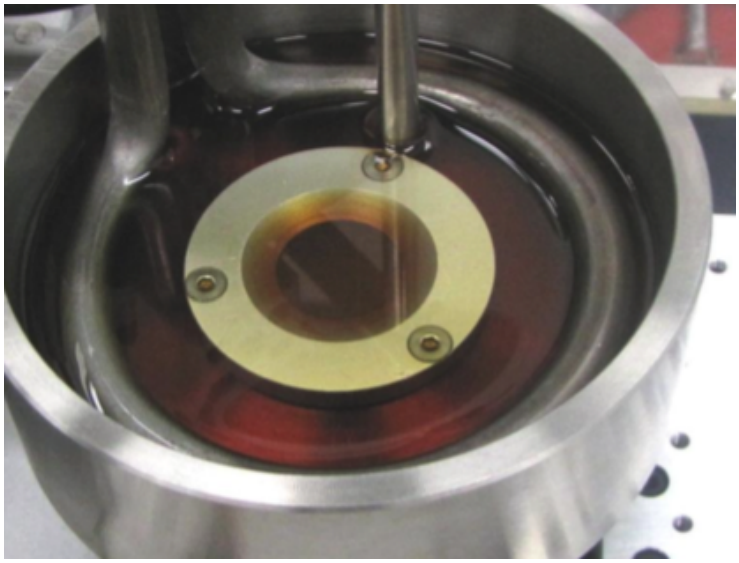

Figure 46: Drilling fluid is added in the sample holder. Pin-on-disk apparatus with an illustrated fluid which covers the sample that is screwed in a fix position and the heating element Instruments [2010].

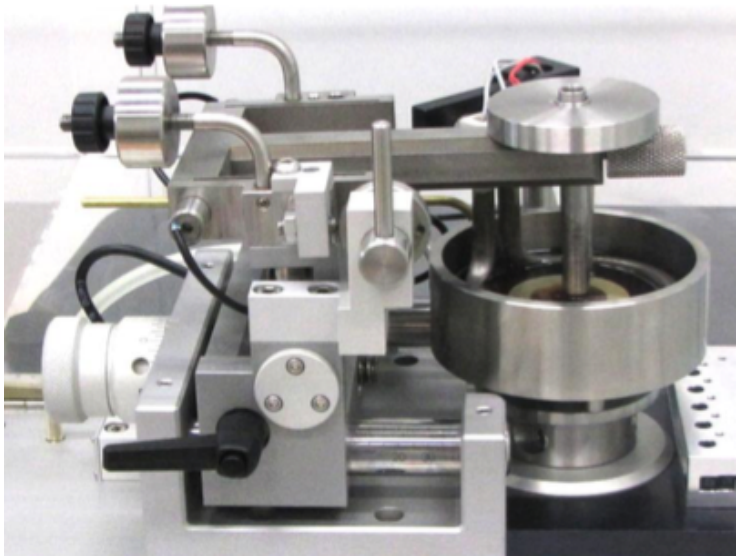

Figure 47: The pin is then lowered and set in position. Added load is put on pin. Pin-on-disk experiment is ready to start. Settings, such as temperature is managed on the computer Instruments [2010].

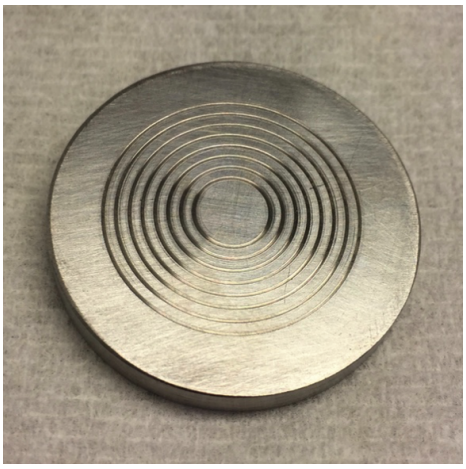

Figure 48: The material sample after the experiment is performed. Each wear track is represented with one observation. The tests starts from $3mm$ radius, and is increased by $1mm$ from each test to $9mm$. The material sample is limited to 7 observations.

5.4 Sources of error

- Changes in humidity and room temperature
- Rheology variations happens over time
- Cleaning of components is not proper
- Small metal particles in drilling fluid due to wear is affecting the results
- High temperatures creates high dehydration that changes the drilling fluid characteristics

The tribology equipment at the University of Stavanger is outdated and not calibrated. This could lead to unwanted errors, and the effects are unknown.

6 Conclusion

In this thesis, we have based our study from the article of Kaarstad et al. [2009], and researched whether the correlation between friction factor and temperature is actually linear or if it should be explained by other functional models. To achieve this, we have done experiments, made certain observations, and performed regression analyses. Our contribution is to investigate the functional form of water based drilling fluid as a lubricator: the friction factor dependency of temperature, which by Kaarstad et al. [2009] was concluded to have linear relationship. We do this by increasing the number of experimental observations and testing different polynomial specifications.

Experimental results

We find that the regression analysis results states that the correlation between the friction factor and the temperature is most accurate and has the most explanatory power with the linear model to explain the gathered experimental data. The R^2, which proxies how much variation in Y is explained by X, tells us that the model explains more of the Y variable for the 3^{rd} degree polynomial model; however, statistically, this is a misguided approach. The reason for this is, when we increase the number of explanatory variables, we automatically explain more of the dependent variable. For this reason, we investigate the precision of the model using the Adjusted R^2 parameter instead. The success of this thesis, in form of results, is concluded to reduce statistical noise in the linear model.

Friction model

The linear model, which is a function of the dependent variable: friction factor, and the independent variable: temperature, is selected to determine the modeled local friction factor in the wellbore. The local friction factor can be implemented in any friction model. In our thesis the friction model of Aadnoy [2006] is used to accentuate the experimental result. By use of a temperature model of Apak.E.C [2006] to determine the local temperature in the wellbore, it emerges that the effect of accurate temperature determination is essential to implement in modeling of torque and drag to avoid overestimation by the correlation with the local friction factor. The results from the experiment could be applied in a simulation friction program, such as Wellplan. Wellplan is used in planning of well program in companies, such as Statoil. Verification of experiment: Real-time data like hook load and torque readings from an actual drilling operation, can be compared to the simulations performed in the Wellplan, which would include the modifications discovered on the friction factor. This approach could present an indication of an improved friction model. This is recommended for future work.

Alternative approaches

We are satisfied with the analysis performed on the models selected: linear, and nonlinear 2^{nd} and 3^{rd} polynomial. However, the statistical analyses in this paper have been constrained by a lack of data. Increasing the sample size in the experiment would add precision to the analysis. If we had more data, then we could perform a different types of regression models. The disadvantage to use a different regression method would be that these are no longer comparable to Kaarstad et al. [2009]. Moreover, the linear trend is defined to be the statistical fit of the selected models, but there still exists the possibility that the other nonlinear polynomials/models could explain the correlation in a nonlinear way. We still have the interesting findings in our results, which matches with Kaarstad et al. [2009], where the friction factor drops after the temperature of $60°C$.

Future work

It would be interesting to investigate the effect of changed density and viscosity in combination with changed temperature to the friction factor for both water-based and oil-based drilling fluid. A research of friction factor between steel and rock would also be an interesting topic to simulate a drilling operation where the drill pipe is in contact with formations under the casing shoe. The result of this thesis will be a success if the pilot research performed would lead to a thorough investigation of the correlation between the friction factor and temperature.

Bibliography

Bernt S Aadnoy. *Mechanics of drilling*. Shaker, 2006.

Bernt S Aadnoy, Mohammad Fazaelizadeh, Geir Hareland, et al. A 3d analytical model for wellbore friction. *Journal of Canadian Petroleum Technology*, 49 (10):25–36, 2010.

Mesfin Belayneh Agonafir. Drill string mechanics special focus on buckling. Chapter 2, 2016.

Al-basheir Khidir Basheir Al-haj, Al-Daow Mohammed Al-Daow, Omer Ahmednour Abdulrahman, and Mohanad Mubarak Yosuf Mubarak. *Modelling of Torque and Drag in Extended Reach Drilling Using Landmark Software*. PhD thesis, Sudan University of Science and Technology, 2015.

Max R Annis et al. High-temperature flow properties of water-base drilling fluids. *Journal of Petroleum Technology*, 19(08):1–074, 1967.

Apak.E.C. A study on heat transfer inside the wellbore during drilling operations. Master's thesis, Middle East Technical University, December 2006.

Bjarne Bennetzen, John Fuller, Erhan Isevcan, Tony Krepp, Richard Meehan, Nelson Mohammed, Jean-Francois Poupeau, and Kumud Sonowal. Extended-reach wells. *Oilfield Rev*, 22(3):4–15, 2010.

BP. Extended reach drilling guidelines. *Chester:P.L.C*, 1996.

WC Browning, AC Perricone, et al. Clay chemistry and drilling fluids. In *Drilling and Rock Mechanics Symposium*. Society of Petroleum Engineers, 1963.

S Jack Burrow. Friction and resistance to sliding in orthodontics: a critical review. *American Journal of Orthodontics and Dentofacial Orthopedics*, 135 (4):442–447, 2009.

DrillScan. Torque & drag & buckling soft-string vs stiff-string models. Technical report, 2013.

Mohammad Fazaelizadeh. *Real Time Torque and Drag Analysis during Directional Drilling*. PhD thesis, University of Calgary, 2013.

Christine Frafjord. Friction factor model and interpretation of real time data. 2013.

ASTM G99-05. Standard testmethod for wear testing with a pin on disk apparatus, 2010.

Erling Grindhaug. The use of alternative materials for drill pipe to extend drilling reach in shallow reservoirs. 2012.

Hendrix. Tension and compression, April 2014. URL http://hendrix2.uoregon.edu/ imamura/102/section2/chapter12.html.

CSM Instruments. *Tribometer User Manual*. CSM instruments SA, Rue de la Gare 4 CH-2034 Peseux (Switzerland), 4.1.i edition, November 2010.

Carolin Jahns. Friction reduction by using nano-fluids in drilling. 2014.

CA Johancsik, DB Friesen, Rapier Dawson, et al. Torque and drag in directional wells-prediction and measurement. *Journal of Petroleum Technology*, 36(06): 987–992, 1984.

Eirik Kaarstad, Bernt Sigve Aadnoy, Tomas Fjelde, et al. A study of temperature dependent friction in wellbore fluids. In *SPE/IADC Drilling Conference and Exhibition*. Society of Petroleum Engineers, 2009.

Ingrid Solberg Kjellevoll. Casing wear: Analysis of field experience and current models. 2013.

UNITED STATES DEPARTMENT OF LABOR. Mud circulation system, 2016.

Colin Mason, David CK Chen, et al. Step changes needed to modernise t&d software. In *SPE/IADC Drilling Conference*. Society of Petroleum Engineers, 2007.

John Edward McCormick, Melissa Anne Frilot, TzuFang Chiu, et al. Torque and drag software model comparison: Impact on application and calibration of field data. In *Brasil Offshore*. Society of Petroleum Engineers, 2011.

Seyed Ahmad Mirhaj, Eirik Kaarstad, and Bernt Sigve Aadnoy. Improvement of torque-and-drag modeling in long-reach wells. *Modern Applied Science*, 5 (5):p10, 2011.

F. Mortensen and A. Brekke. Extended reach drilling; an analytical approach of calculating the maximum length of a well. May 2014. Bachelor Thesis.

Robello Samuel. Friction factors: What are they for torque, drag, vibration, bottom hole assembly and transient surge/swab analyses? *Journal of Petroleum Science and Engineering*, 73(3):258–266, 2010.

D Summers-Smith. Handbook of lubrication: Theory and practice of tribology: Volume 2: Theory and design, 1984.

Wikipedia-Friction. Friction, 2016. URL https://en.wikipedia.org/wiki/Friction.

Wikipedia-Geothermal. Geothermal gradient. 2016. https://en.wikipedia.org/wiki/Geothermalgradient.

Andrew Wu, Geir Hareland, and Mohammad Fazaelizadeh. Torque & drag analysis using finite element method. *Modern Applied Science*, 5(6):13, 2011.

List of Figures

List of Tables

Appendix

CSM Instruments SA
Rue de la Gare 4
2034 Peseux - Switzerland

Glydril.v.1

Glydril.v.1

Tribo measurement

Tribo parameters

Acquisition
Radius : 4.03 [mm]
Lin. speed : 3.57 [cm/s]
Normal load : 10.00 [N]
Stop condit. : 20.00 [m]
Or μ > 1.00
Effective stop : meters
Acquisition rate : 5.0 [hz]

Sample
-Substrate : Steel
-Cleaning : Ethanol
-Supplier : UiS workshop

Static partner
-Coating : bent
-Substrate : 100Cr6
-Cleaning : Ethanol
-Supplier : CSM Instruments
-Dimension : 6.00 [mm]
-Geometry : Ball

Environment
Temperature : 30.00 [°C]
Atmosphere : 22.1
Humidity : 50.00 [%]
Lubricant : Glydril
-Volume : 150.00 [ml]
-Application : Liquid covers sample and

Sample
Worn track section : 0.0 μm2
Young's modulus : 0.0 gpa
Poisson ratio : 0.000

Static partner
Worn cap diameter : 0.0 μm
Young's modulus : 0.0 gpa
Poisson ratio : 0.000

Calculations
Sample wear rate : 0 mm3/n/m
Partner wear rate : 0 mm3/n/m
Max Herzian stress : 0 gpa

Curve

Start : 0.227 min : 0.155 max : 0.325 mean : 0.256 std. dev. : 0.020

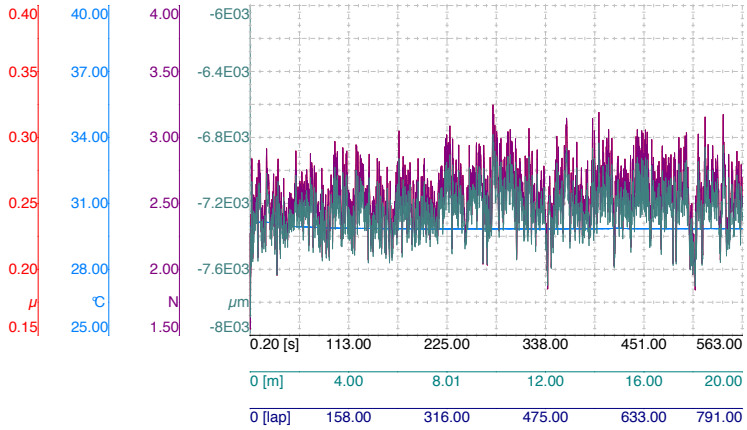

Tribo measurement

Tribo parameters

Acquisition	Sample	Static partner	Environment
Radius : 9.01 [mm]	-Substrate : Steel	-Coating : bent	Temperature : 40.00 [°C]
Lin. speed : 7.93 [cm/s]	-Cleaning : Ethanol	-Substrate : 100Cr6	Atmosphere : 22.1
Normal load : 10.00 [N]	-Supplier : UiS Workshop	-Cleaning : Ethanol	Humidity : 50.00 [%]
Stop condit. : 20.00 [m]		-Supplier : CSM	Lubricant : Glydril
Or μ > 1.00		-Dimension : 6.00 [mm]	-Volume : 150.00 [ml]
Effective stop : meters		-Geometry : Ball	-Application : Liquid cov. sample
Acquisition rate : 5.0 [hz]			

Sample	Static partner	Calculations
Worn track section : 0.0 μm2	Worn cap diameter : 0.0 μm	Sample wear rate : 0 mm3/n/m
Young's modulus : 0.0 gpa	Young's modulus : 0.0 gpa	Partner wear rate : 0 mm3/n/m
Poisson ratio : 0.000	Poisson ratio : 0.000	Max Herzian stress : 0 gpa

Curve

Start : 0.412 min : 0.184 max : 0.412 mean : 0.272 std. dev. : 0.030

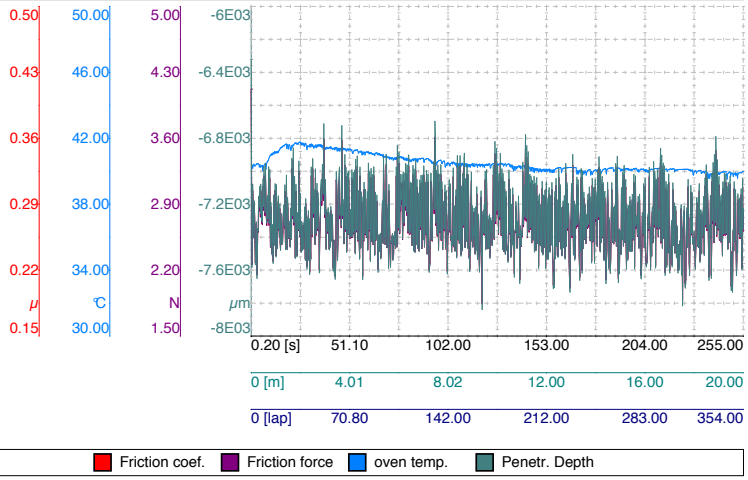

Tribo measurement

Tribo parameters

Acquisition
Radius : 6.03 [mm]
Lin. speed : 5.37 [cm/s]
Normal load : 10.00 [N]
Stop condit. : 20.00 [m]
Or μ > 1.00
Effective stop : meters
Acquisition rate : 5.0 [hz]

Sample
-Substrate : Steel
-Cleaning : Ethanol
-Supplier : UiS Workshop

Static partner
-Coating : bent
-Substrate : 100Cr6
-Cleaning : Ethanol
-Supplier : CSM
-Dimension : 6.00 [mm]
-Geometry : Ball

Environment
Temperature : 50.00 [°C]
Atmosphere : 22.1
Humidity : 50.00 [%]
Lubricant : Glydril
-Volume : 150.00 [ml]
-Application : Liquid cov. sample

Sample
Worn track section : 0.0 μm2
Young's modulus : 0.0 gpa
Poisson ratio : 0.000

Static partner
Worn cap diameter : 0.0 μm
Young's modulus : 0.0 gpa
Poisson ratio : 0.000

Calculations
Sample wear rate : 0 mm3/n/m
Partner wear rate : 0 mm3/n/m
Max Herzian stress : 0 gpa

Curve

Start : 0.250 min : 0.214 max : 0.394 mean : 0.304 std. dev. : 0.027

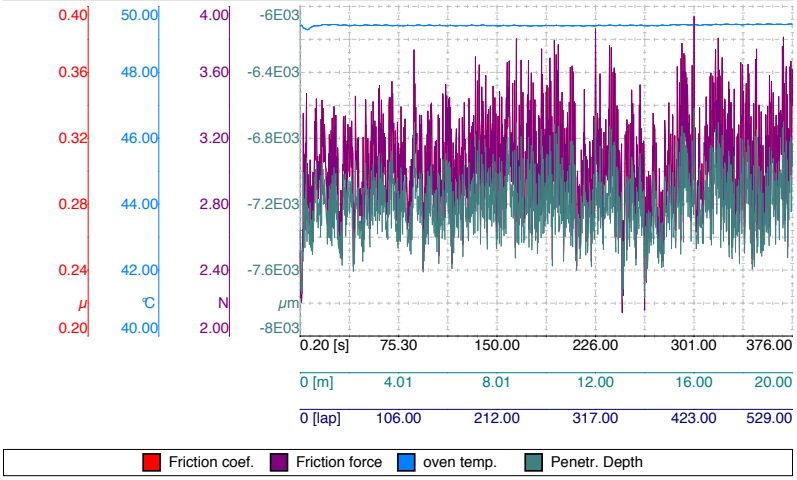

Tribo measurement

Tribo parameters

Acquisition
Radius : 9.05 [mm]
Lin. speed : 7.96 [cm/s]
Normal load : 10.00 [N]
Stop condit. : 20.00 [m]
Or $\mu > 1.00$
Effective stop : meters
Acquisition rate : 5.0 [hz]

Sample
-Substrate : Steel
-Cleaning : Ethanol
-Supplier : UiS Workshop

Static partner
-Coating : bent
-Substrate : 100Cr6
-Cleaning : Ethanol
-Supplier : CSM
-Dimension : 6.00 [mm]
-Geometry : Ball

Environment
Temperature : 62.00 [°C]
Atmosphere : 22.1
Humidity : 50.00 [%]
Lubricant : Glydril
-Volume : 150.00 [ml]
-Application : Liquid cov. sample

Sample
Worn track section : 0.0 μm2
Young's modulus : 0.0 gpa
Poisson ratio : 0.000

Static partner
Worn cap diameter : 0.0 μm
Young's modulus : 0.0 gpa
Poisson ratio : 0.000

Calculations
Sample wear rate : 0 mm3/n/m
Partner wear rate : 0 mm3/n/m
Max Herzian stress : 0 gpa

Curve

Start : 0.301 min : 0.213 max : 0.477 mean : 0.345 std. dev. : 0.042

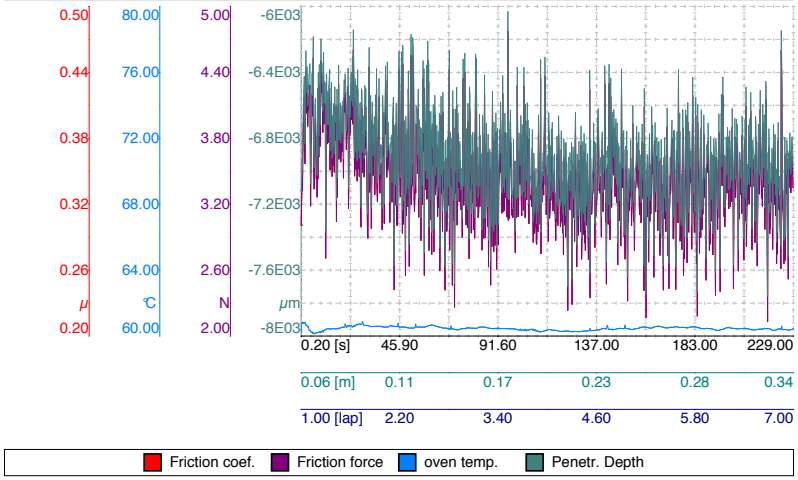

Tribo measurement

Tribo parameters

Acquisition
Radius : 2.99 [mm]
Lin. speed : 2.63 [cm/s]
Normal load : 10.00 [N]
Stop condit. : 20.00 [m]
Or μ > 1.00
Effective stop : meters
Acquisition rate : 5.0 [hz]

Sample
-Substrate : Steel
-Cleaning : Ethanol
-Supplier : UiS Workshop

Static partner
-Coating : bent
-Substrate : 100Cr6
-Cleaning : Ethanol
-Supplier : CSM
-Dimension : 6.00 [mm]
-Geometry : Ball

Environment
Temperature : 72.00 [°C]
Atmosphere : 22.1
Humidity : 50.00 [%]
Lubricant : Glydril
-Volume : 150.00 [ml]
-Application : Liquid cov. sample

Sample
Worn track section : 0.0 μm2
Young's modulus : 0.0 gpa
Poisson ratio : 0.000

Static partner
Worn cap diameter : 0.0 μm
Young's modulus : 0.0 gpa
Poisson ratio : 0.000

Calculations
Sample wear rate : 0 mm3/n/m
Partner wear rate : 0 mm3/n/m
Max Herzian stress : 0 gpa

Curve

Start : 0.298 min : 0.241 max : 0.387 mean : 0.300 std. dev. : 0.023